

Mineralogy, Geochemistry, and Sr–Nd–Pb Isotope Systematics of Late Cenozoic Basanites of the Borozdin Bald Mountain (Khentei Ridge, Southern Transbaikalia)

A.Ya. Medvedev^{a,✉}, M.A. Gornova^a, S.I. Dril'^a, A.A. Karimov^a, V.A. Belyaev^a,
A.V. Ivanov^b, E.I. Demonterova^b

^a Vinogradov Institute of Geochemistry, Siberian Branch of the Russian Academy of Sciences, ul. Favorskogo 1a, Irkutsk, 664033, Russia

^b Institute of the Earth's Crust, Siberian Branch of the Russian Academy of Sciences, ul. Lermontova 128, Irkutsk, 664033, Russia

Received 12 March 2019; received in revised form 21 May; accepted 10 October 2019

Abstract—We have estimated the P – T conditions of formation of basaltoid melts: $P = 1.15$ – 1.06 GPa and $T = 1379$ – 1293 °C. Olivine pyroxenites (Ol + Cpx + Grt) are assumed to be a mantle source for nepheline-normative basanitic melts. During ascent, the melt trapped mantle xenoliths, which were disintegrated into olivine and augite xenocrysts. A decrease in pressure and temperature led to the crystallization of highly magnesian (Mg# = 86) olivine and diopside and Timgt + Ilm ± Pl phenocrysts. Then, the Ol + Cpx + Timgt + Pl microlite paragenesis formed. Alkaline aluminosilicates (acid plagioclase + nepheline + leucite) were the last to crystallize in the rock interstices. The presence of residual glass indicates that the last stage of crystallization took place under subsurface conditions. The volcanic area of southern Transbaikalia (Khentei Ridge) resulted, most likely, from the mantle plume impact on the lithosphere. The age of this area is estimated at 3.51 Ma. PREMA was the main mantle source for these volcanics, and the contribution of HIMU was strongly subordinate. In geochemical features the studied volcanics correspond to mafic rocks of oceanic islands. They are similar in composition to alkali basalts of the South Baikal volcanic area.

Keywords: basalts, pressure, temperature, parental melt, crystallization sequence, plume, Pb–Nd–Sr isotopy

INTRODUCTION

In the late Cenozoic, volcanism was widely manifested in the southern framing of the Siberian craton. Its products formed a number of fields of different sizes and durations of formation (Laverov, 2008). The volcanic fields extend from the Udokan lava plateau in the north via the South Baikal and South Hangayn areas to the Dariganga Plateau (Mongolia) in the south and form the Central Asian volcanic province (CAVP) (Yarmolyuk et al., 1995). Several stages of magmatic activity (from 34 Ma to recent time) were established in almost all volcanic areas (Yarmolyuk et al., 1998, 2003, 2011). In addition, all areas are characterized by a predominance of mafic lavas, mostly of alkaline and subalkaline types. Almost all Cenozoic volcanics are localized in rift structures.

The Baikal Rift Zone (BRZ) is the largest rift structure in Central Asia (Kiselev et al., 1979; Kovalenko et al., 1999, 2009; Logachev, 2003; Voronstov and Yarmolyuk, 2004; Buslov, 2012). Near the southwestern flank of the BRZ there is the South Baikal volcanic area (SBVA) (350×

450 km), where several stages of magmatism, from late Oligocene (34–24 Ma) to late Pliocene–Pleistocene–Holocene (<3 Ma) (Yarmolyuk et al., 2001), were recognized (Yarmolyuk et al., 2001). The SBVA volcanics are mafic alkaline rocks, from potassic trachybasalts to basanites and hawaiites (Yarmolyuk et al., 2003). In geochemical features they are similar to oceanic-island basalts.

Southern Transbaikalia is one of the areas of Cenozoic volcanics not related to rifting, but such rocks are less spread here as compared with the SBVA. Cenozoic alkali basalts with a great number of xenoliths have been long known in the Khentei Ridge in southern Transbaikalia. They occur as lava flows and nappes of small area and thickness in the headwaters of the Chikoi, Chikokon, and Burkal rivers. The first data on these volcanics were reported by Kostyakov et al. (1969). Later, the hosted xenoliths, including garnet and spinel lherzolites, were examined (Rasskazov, 1987; Ashchepkov et al., 1996; Litasov and Taniguchi, 2002).

The chemical composition of the basaltoids has been poorly studied. We found results of only three wet-chemistry analyses of these rocks (Kostyakov et al., 1969; Rasskazov, 1987) and no data on the composition of their minerals. The goal of this research was to determine the composition of parental magmas, the isotope sources, and the P – T condi-

✉ Corresponding author.

E-mail address: amedv@igc.irk.ru (A.Ya. Medvedev)

tions of formation of basanites of the Borozdin Bald Mountain. For this purpose we studied the composition of minerals, obtained the first data on the isotope composition of rocks, and determined the absolute age of volcanism.

ANALYTICAL METHODS

Analyses were carried out for sample fragments without visible xenoliths. The compositions of minerals were determined by electron probe microanalysis (EPMA) on a JXA-8200 (JEOL Ltd., Japan) probe. The contents of rock-forming elements were measured by X-ray fluorescence analysis on a SRM-25 (ZAO Nauchpribor, Orel) multichannel X-ray spectrometer according to the technique of Afonin et al. (1984). The spectrometer was calibrated against the ST-1A (trapp, Russia) and JB-1 (basalt, Japan) standard samples (Finkel'shtein et al., 1984). The contents of trace elements were determined by ICP MS on an ELEMENT-2 (Finnigan MAT, Germany) double-focusing mass spectrometer with a magnetic sector. The analytical techniques are given elsewhere (Mysovskaya et al., 2009; Saibatalova et al., 2010).

The samples for isotope analysis were chemically prepared in clean chemical rooms of the Common Use Center for Isotope-Geochemical Studies of the Institute of Geochemistry, Irkutsk. The isotope composition of Sr and the contents of Rb and Sr were determined by the isotope dilution method, using a mixed $^{85}\text{Rb} + ^{84}\text{Sr}$ tracer. The isotope composition of Nd and the contents of Nd and Sm were determined by the isotope dilution method, using a mixed $^{149}\text{Sm} + ^{150}\text{Nd}$ tracer.

The isotope compositions of Sr and Nd were measured on a Finnigan MAT-262 seven-channel mass spectrometer at the Center for Geodynamics and Geochronology of the Institute of the Earth's Crust, Irkutsk. The measured isotope ratios were normalized to $^{88}\text{Sr}/^{86}\text{Sr} = 8.37521$. The validity of the obtained Sr isotope data was estimated by analysis of the NBS-987 and BCR-2 standard samples, which yielded $^{87}\text{Sr}/^{86}\text{Sr} = 0.710254 \pm 7$ (2SD, $n = 45$) and $^{87}\text{Sr}/^{86}\text{Sr} = 0.705011 \pm 14$ (2SD, $n = 7$), respectively. The validity of the obtained Nd isotope data was estimated by analysis of the JNdi-1 and BCR-2 standard samples, which yielded $^{143}\text{Nd}/^{144}\text{Nd} = 0.512107 \pm 4$ (2SD, $n = 35$) and $^{143}\text{Nd}/^{144}\text{Nd} = 0.512629 \pm 8$ (2SD, $n = 18$), respectively.

The isotope composition of Pb in the rocks was measured on a Finnigan MAT-262 mass spectrometer. Correction for mass discrimination was made using the double isotope dilution method. The isotope composition was determined in the sample and in its mixture with a $^{207}\text{Pb} + ^{204}\text{Pb}$ tracer. The $^{207}\text{Pb}/^{204}\text{Pb}$ ratio in the tracer was close to 1 in accordance with recommendations (Rudge et al., 2009). The validity of the determined isotope composition was estimated by analysis of the NBS-981 standard sample with the following normalized isotope ratios: $^{208}\text{Pb}/^{204}\text{Pb} = 36.7029 \pm 35$; $^{207}\text{Pb}/^{204}\text{Pb} = 15.4911 \pm 16$; and $^{206}\text{Pb}/^{204}\text{Pb} = 16.9372 \pm 6$ (2SD, $n = 22$).

The $^{40}\text{Ar}/^{39}\text{Ar}$ isotopic age was determined by the step heating method with measurement of the isotope composition of released argon on an ARGUS VI mass spectrometer (Thermo Scientific, Great Britain) at the Center for Geodynamics and Geochronology of the Institute of the Earth's Crust, Irkutsk. The analytical technique is described in detail by Ivanov et al. (2017).

THE GEOLOGIC POSITION AND PETROGRAPHY OF THE STUDIED ROCKS

The Borozdin Bald Mountain is located in the headstream of the Borozdinaya and Kharchevka rivers, right tributaries of the Burkal River (Fig. 1) (Kostyakov et al., 1969). The peak of this bald mountain is composed of compact black and dark gray volcanics, which overlie the rocks of the Ingoda Formation (C_{1-2}). The volcanics contain mantle xenoliths of spinel and garnet lherzolites composed of high-Mg olivine, augite, spinel, and relict garnet as well as olivine and clinopyroxene xenocrysts. The rocks were sampled from massive volcanics of bedrock exposures at the peak of the Borozdin Bald Mountain. For study we chose samples without visible xenoliths.

The sampled rocks contain large inclusions of olivine and clinopyroxene; their total content varies from 0 to 4–5 vol.%. Massive volcanics are composed of varieties of porphyritic and aphyric textures (Fig. 2). As shown below, the porphyritic texture is due to large phenocrysts and xenocrysts of olivine (0.5–1.0 mm, Fig. 2) and clinopyroxene (0.4–0.5 mm, Fig. 2). The large pyroxene grains are much scarcer than the large olivine grains and amount to ~1.5 vol.%. Seldom, plagioclase phenocrysts ≤ 0.3 mm in size (sample B11/3) are found. Both the phenocrysts and the xenocrysts of olivine and clinopyroxene are fresh. The rock groundmass is of intersertal texture and is formed by fine grains of olivine (≤ 0.03 mm), clinopyroxene (≤ 0.01 mm), ore minerals 40–50 μm in size, thin plagioclase laths (150–200 μm), and a finely crystallized aggregate with glass relics. According to the probe microanalysis results, the aggregate contains nepheline, leucite, apatite, and felsic-plagioclase microlites no larger than 50 μm . The presence of glass relics suggests that the final stage of crystallization proceeded in subsurface conditions. Postmagmatic alterations are minor, as evidenced from the low LOI values.

THE AGE

We performed Ar/Ar dating of the fine-crystalline basaltoids. The Ar release spectrum of the sample B15 shows excess argon, which is present, most likely, in xenogenic pyroxenes (Fig. 3). This is indicated by the significant increase in Ca/K with increasing temperature (Table 1), when a K-containing phase (leucite) is exhausted and a Ca-containing phase (clinopyroxene) is involved in melting (Buikin

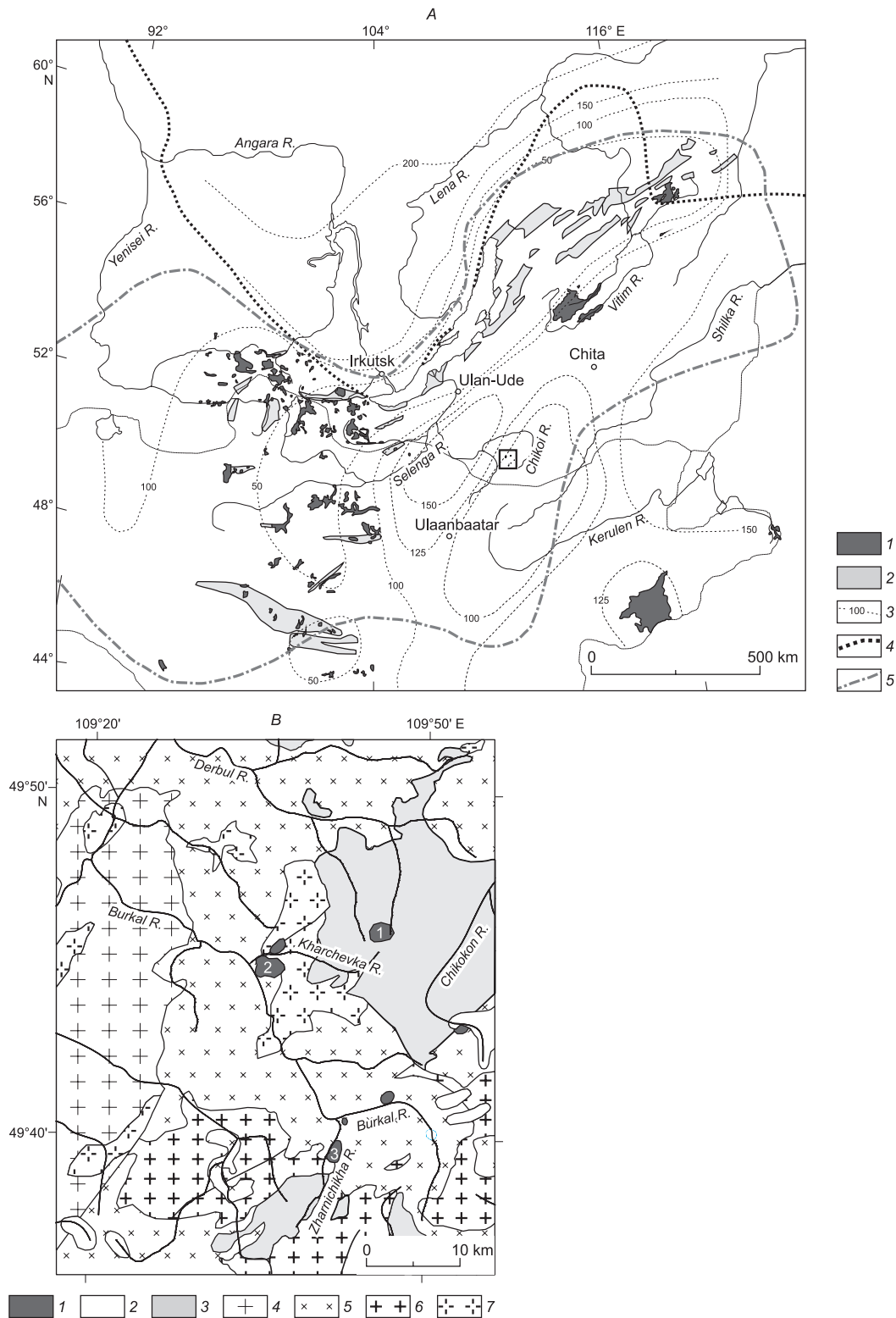


Fig. 1. Position of Cenozoic volcanics in the Baikal–Mongolian region (Litasov and Taniguchi, 2002) (A); geological map of the area of Cenozoic alkali basalts of the Dauria–Khentei Ridge, simplified and supplemented after State... (2012) (B). A: 1, Cenozoic volcanics; 2, Cenozoic sedimentary basins and depressions; 3, lithosphere thickness, km (Zorin et al., 1990); 4, border of the Siberian craton; 5, border of the area of anomalous low-velocity mantle (Zorin and Rogozhina, 1978). Rectangle marks the position of alkali basalts of the Dauria–Khentei Ridge; B: 1, late Cenozoic alkali basalts; 2, Quaternary fluvioglacial deposits; 3, Carboniferous deposits of the Ingoda Group; 4, granitoids of the Malkhan complex (PZ₁); 5, granitoids of the Daur complex (P₁); 6, granitoids of the Kyra complex (J_{1–2}); 7, granitoids of the Asakan–Shumilovka complex (J_{2–3}). Numerals mark outcrops of Cenozoic alkali basalts: 1, Borozdin Bald Mountain; 2, Kharchevka; 3, Zharnichikha.

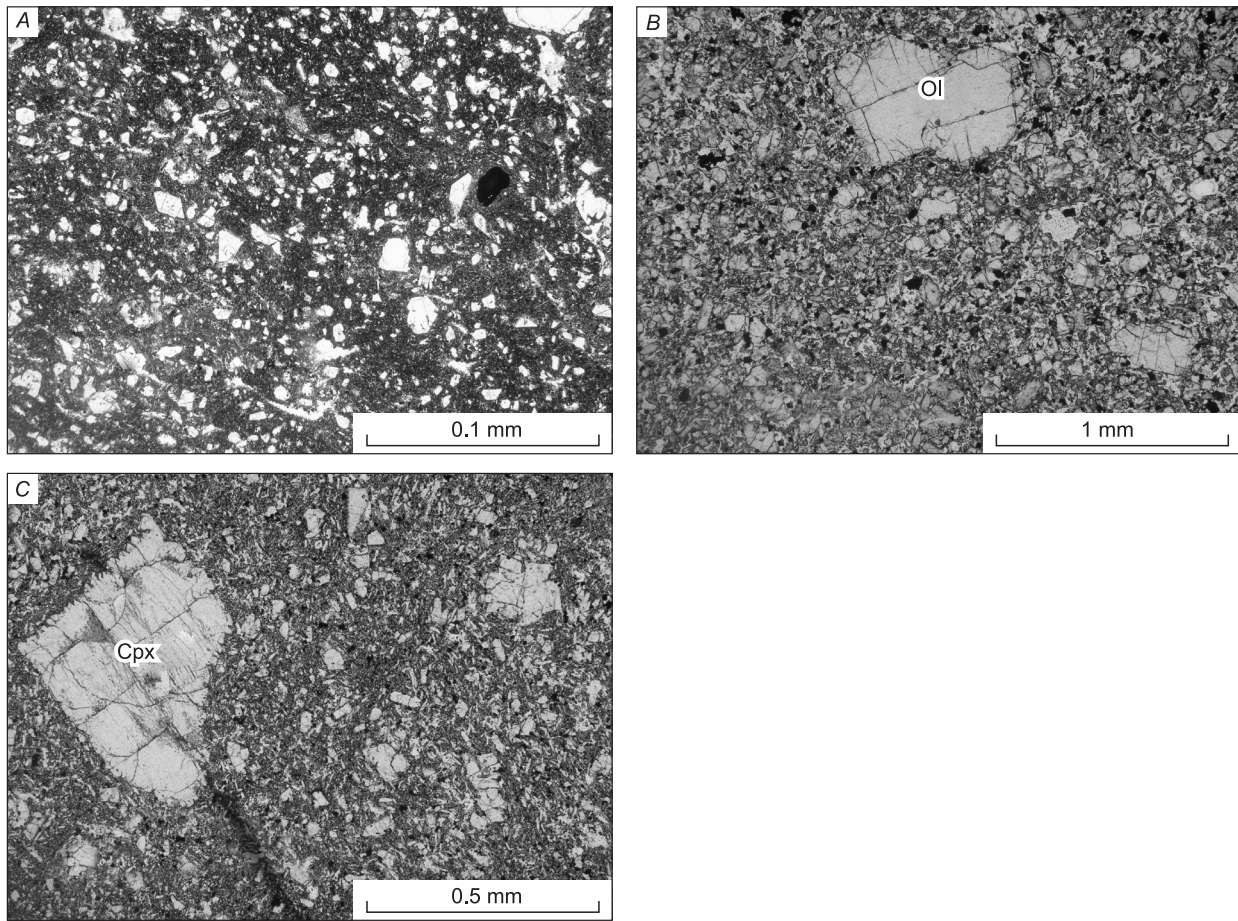


Fig. 2. Thin-section photomicrographs. *A*, Aphyric volcanic rock, sample B11/2, white is fine olivine grains (Ol); *B*, porphyritic volcanic rock with olivine xenocryst, sample B26; *C*, porphyritic volcanic rock with clinopyroxene xenocryst (Cpx), sample B15.

et al., 2010). Thus, the age of the sample is determined from two low-temperature steps. Moreover, olivine might contain microinclusions that crystallized from a basanitic melt (Ivanov et al., 2018). The obtained date of 3.51 ± 0.27 Ma is reliably the upper temporal bound of volcanism or, most likely, corresponds to the time of formation of basanites. The age of the complete melting of the sample, i.e., its K–Ar age, is 7.18 ± 0.37 Ma. Earlier, K–Ar dates of 7.9 and

5.7 Ma were obtained for two melanephelinite samples from the same area, with no analytical error mentioned (Polyakov and Bagdasar’yan, 1986). Obviously, they show an older age because of the presence of excess argon in xenogenic pyroxene in these samples.

MINERAL COMPOSITION

Olivines. Table 2 lists the representative compositions of olivines of three morphologic varieties: (1) ellipsoidal or irregular grains with wavy edges, up to 1 mm in size (Fig. 4), (2) subhedral grains up to 0.4 mm in size, and (3) fine euhedral grains smaller than 50 μm (Fig. 5). Figure 6 shows variations in the compositions of olivine grains of different sizes and shapes. The Mg# value of olivines varies over a wide range of values and gradually decreases from core to rim in large grains. A positive Fo–NiO correlation and a negative Fo–CaO correlation are observed. The content of CaO in the cores of zoned olivine grains is <0.2 wt.% and is higher, within 0.20–0.34 wt.%, in the rims of large olivine grains and in the phenocrysts with Mg# ≈ 0.77.

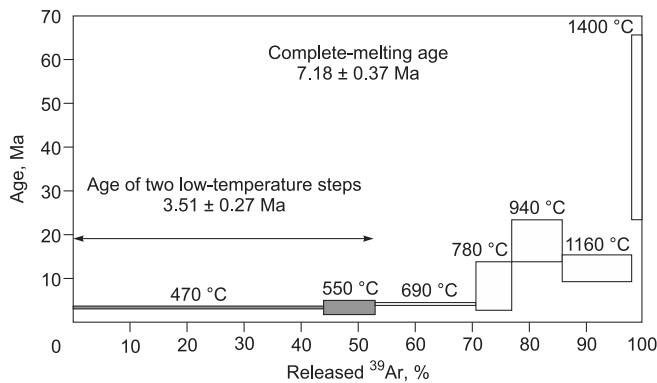


Fig. 3. Results of $^{40}\text{Ar}/^{39}\text{Ar}$ dating of the sample B15.

Table 1. Results of $^{40}\text{Ar}/^{39}\text{Ar}$ dating

| Step | T, °C | ^{40}Ar | $\pm 1\sigma$ | ^{39}Ar | $\pm 1\sigma$ | ^{38}Ar | $\pm 1\sigma$ | ^{37}Ar | $\pm 1\sigma$ | ^{36}Ar | $\pm 1\sigma$ | Ca/K | $^{40}\text{Ar}_{\text{rad}}/^{39}\text{Ar}$ | $\pm 1\sigma$ | Age, Ma | $\pm 2\sigma$ |
|------|-------|------------------|---------------|------------------|---------------|------------------|---------------|------------------|---------------|------------------|---------------|--------|--|---------------|---------|---------------|
| 1 | 468 | 949.10 | 3.61 | 888.85 | 3.03 | 15.21 | 0.22 | 86.22 | 2.76 | 1.903 | 0.196 | 0.36 | 0.43 | 0.02 | 3.51 | 0.27 |
| 2 | 552 | 186.38 | 0.80 | 181.70 | 0.79 | 5.79 | 0.23 | 160.16 | 2.77 | 0.369 | 0.218 | 3.26 | 0.42 | 0.09 | 3.43 | 1.51 |
| 3 | 687 | 1 656.95 | 5.67 | 354.79 | 1.29 | 6.76 | 0.21 | 606.86 | 3.32 | 4.918 | 0.202 | 6.33 | 0.53 | 0.01 | 4.35 | 0.17 |
| 4 | 783 | 167.37 | 0.71 | 129.79 | 0.61 | 2.00 | 0.19 | 275.40 | 2.80 | 0.111 | 0.209 | 7.85 | 1.03 | 0.32 | 8.45 | 5.27 |
| 5 | 936 | 460.15 | 1.68 | 174.98 | 0.79 | 3.73 | 0.23 | 1 724.08 | 6.57 | 0.204 | 0.226 | 36.46 | 2.28 | 0.30 | 18.60 | 4.82 |
| 6 | 1156 | 469.14 | 1.73 | 249.23 | 0.97 | 6.05 | 0.23 | 7 212.48 | 25.12 | 0.310 | 0.238 | 107.07 | 1.51 | 0.19 | 12.34 | 3.13 |
| 7 | 1396 | 229.44 | 0.84 | 39.32 | 0.43 | 0.80 | 0.19 | 1 864.68 | 7.03 | 0.045 | 0.193 | 175.45 | 5.49 | 1.30 | 44.48 | 21.09 |

Table 2. Results of representative analyses of olivine phenocrysts

| Component | B15 | | | | B11/2 | | | | | |
|-------------------------|------------------------|-------------------|-------|-------|-------|-------------------|-------|-------|-------|-------|
| | Xenogenic olivine Ol 1 | | | | | | | | | |
| | Large zoned grain | | | | | | | | | |
| | core | intermediate zone | | rim | core | intermediate zone | | rim | | |
| SiO ₂ , wt.% | 40.68 | 41.72 | 40.63 | 38.98 | 41.02 | 40.38 | 40.51 | 40.48 | 39.24 | 38.57 |
| FeO* | 8.93 | 8.91 | 17.15 | 18.47 | 9.22 | 9.22 | 9.53 | 13.11 | 15.75 | 21.03 |
| MnO | 0.13 | 0.12 | 0.36 | 0.40 | 0.10 | 0.10 | 0.10 | 0.19 | 0.28 | 0.41 |
| MgO | 49.26 | 48.64 | 42.94 | 42.16 | 50.08 | 50.08 | 50.17 | 46.99 | 44.92 | 39.48 |
| CaO | 0.13 | 0.12 | 0.17 | 0.21 | 0.13 | 0.13 | 0.09 | 0.07 | 0.15 | 0.29 |
| NiO | 0.39 | 0.40 | 0.24 | 0.18 | 0.36 | 0.36 | 0.34 | 0.33 | 0.29 | 0.15 |
| Total | 99.52 | 99.61 | 101.5 | 100.4 | 100.9 | 100.3 | 100.7 | 101.2 | 100.6 | 100.3 |
| Mg# | 0.91 | 0.90 | 0.82 | 0.80 | 0.91 | 0.91 | 0.90 | 0.86 | 0.84 | 0.77 |

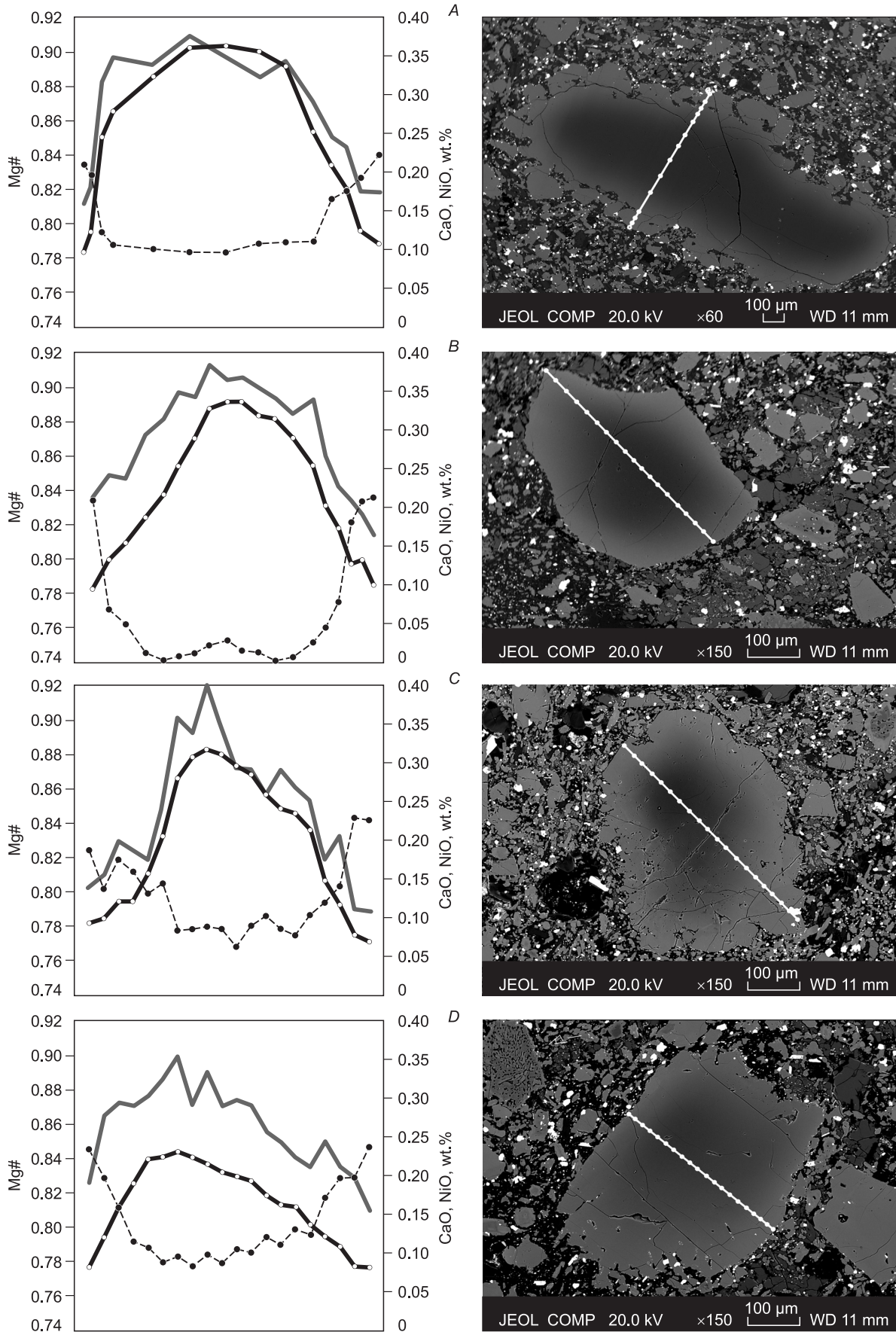
| Component | B04 | | | | B26 | | | | | |
|-------------------------|---|-------|-------------------|-------|------------------------|--------|-------------------|-------|-------|-------|
| | Olivines of generation I (basaltic), Ol 2 | | | | | | | | | |
| | Large zoned grain | | | | Fine homogeneous grain | | | | | |
| | core | core | intermediate zone | | rim | core | intermediate zone | | rim | |
| SiO ₂ , wt.% | 39.01 | 40.12 | 39.05 | 38.53 | 39.28 | 38.76 | 38.27 | 37.96 | 38.01 | 38.41 |
| FeO* | 13.54 | 14.32 | 15.80 | 18.37 | 18.57 | 19.37 | 21.28 | 20.98 | 21.02 | 21.10 |
| MnO | 0.17 | 0.19 | 0.19 | 0.30 | 0.30 | 0.34 | 0.40 | 0.41 | 0.39 | 0.43 |
| MgO | 46.96 | 46.19 | 44.26 | 42.62 | 42.01 | 41.85 | 40.31 | 40.53 | 40.37 | 40.13 |
| CaO | 0.19 | 0.19 | 0.22 | 0.22 | 0.22 | 0.26 | 0.27 | 0.26 | 0.27 | 0.27 |
| NiO | 0.25 | 0.20 | 0.20 | 0.19 | 0.16 | 0.16 | 0.15 | 0.14 | 0.13 | 0.14 |
| Total | 100.1 | 101.2 | 99.72 | 101.2 | 100.5 | 100.74 | 100.7 | 100.3 | 100.2 | 100.5 |
| Mg# | 0.86 | 0.85 | 0.83 | 0.79 | 0.80 | 0.79 | 0.77 | 0.77 | 0.77 | 0.77 |

Note. Electron probe microanalyses were carried out by O.Yu. Belozerova. Mg# = Mg/(Mg + Fe²⁺), mol.%. Hereafter, FeO* is total iron.

Olivine grains with Mg# > 0.90 in the core have rounded wavy edges (Fig. 4A). Similar outlines of olivine grains are observed in the experiments on the interaction of peridotites with SiO₂-undersaturated basaltic melts (Shaw and Dingwell, 2008). The grains are zoned: The NiO content and Mg# decrease and the CaO content increases from core to edge (Fig. 4A). The core has a zone of homogeneous composition typical of equilibrium olivines of mantle peridotites. The CaO content in this zone is still the same as in mantle peridotite, whereas the NiO and Fo contents are lower. This phenomenon might be due to the different rates

of element diffusion at the olivine–basaltic contact. The lower rate of CaO diffusion was established during the modeling of assimilation of olivine xenocrysts by basalts, based on the observed olivine composition trends (Costa and Dungan, 2005). Dissolution of crystals can lead to their rounded shape (Donaldson, 1985). The diffusion zoning in olivines indicates that the rate of dissolution was lower than the rate of diffusion (Liang, 2000). These grains are obviously xenogenic olivines (Ol 1) of mantle peridotites.

Euhedral and subhedral olivines show different Fo, NiO, and CaO concentration profiles: The core zone of homoge-



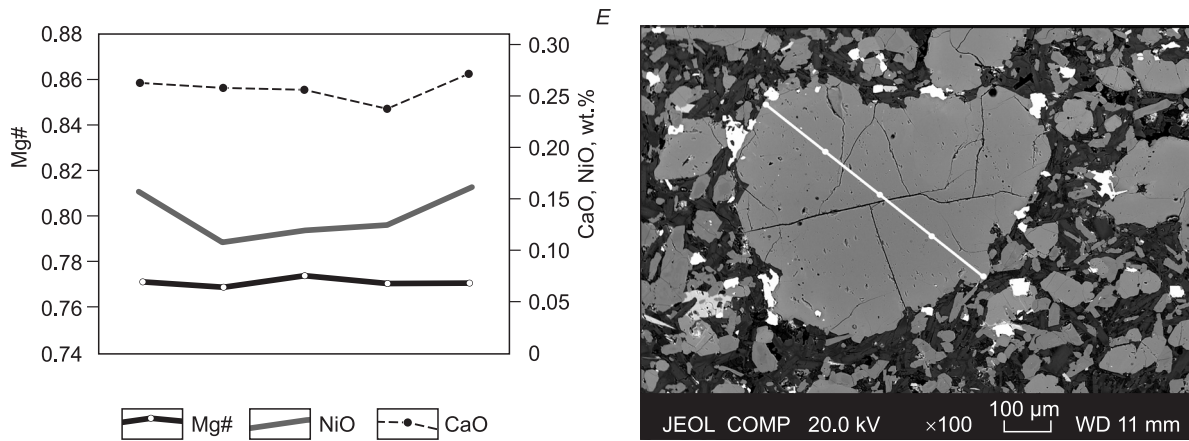


Fig. 4. CaO and NiO contents vs Mg# of olivine and BSE images of xenogenic olivines (Superprobe JXA-8200 (JEOL Ltd, Japan) electron microprobe; accelerating voltage of 20 kV, beam current of 20 nA, and beam diameter of 1 μm). A, BB1; B, B26; C, B15; D, B26; E, B26. Here and in Fig. 5, white lines and dots mark the scanning profiles and analysis points, respectively.

neous composition has close contents of all elements; a decrease in the Fo and NiO contents to the edge of the grain is accompanied by an increase in the CaO content. These profiles might be due to crystallization of olivine from melt (Fig. 5). In the core of these olivine grains (Ol 2) Mg# varies from 0.86 to 0.81, the CaO content, from 0.10 to 0.18, and the NiO content, from 0.19 to 0.32 wt.%. The fine homogeneous euhedral olivine grains (Ol 3) have Mg# \approx 0.77, CaO \approx 0.25 wt.%, and NiO \approx 0.15 wt.%. In composition they are similar to the edges of zoned xenocrysts and phenocrysts (Fig. 6). Accordingly, these olivines crystallized from the last portion of basaltic melt.

Thus, we discovered several varieties of olivine: xenogenic (Ol 1), basaltic (Ol 2, generation I), and fine homogeneous grains in the groundmass (Ol 3, generation II). Note that the formation of several generations of olivine from basaltic melt is often observed (Al'mukhamedov et al., 1983, 1985; Zolotukhin et al., 1996).

Pyroxenes. All samples contain phenocrysts (<500 μm in size) and megacrysts (0.7 mm) of clinopyroxene. Fine grains of pyroxene are also found in the rock groundmass. Results of representative analyses of these pyroxenes are given in Table 3. The phenocrysts are diopsides (Cpx 2); the large ones are zoned, with Mg# = 0.82–0.74. The contents

Table 3. Results of representative analyses of clinopyroxene phenocrysts

| Component | B11-2 | | B15 | | | | | B26 | | | | | |
|--------------------------------|-------|-------|--------|--------|------------------------------|--------|--------|------------------------------|-------|-------|--------|--------|--------|
| | Cpx 1 | | Cpx 1 | | Fine grain of the groundmass | Cpx 2 | | Fine grain of the groundmass | | | | | |
| | core | rim | core | rim | | rim | core | core | Cpx 1 | | | | |
| SiO ₂ , wt.% | 53.30 | 52.87 | 52.23 | 51.63 | 50.10 | 50.38 | 52.60 | 50.98 | 46.88 | 49.88 | 47.68 | 51.97 | 53.84 |
| TiO ₂ | 0.35 | 0.41 | 0.89 | 1.81 | 2.50 | 2.71 | 1.11 | 1.01 | 3.58 | 3.20 | 2.99 | 0.95 | 0.58 |
| Al ₂ O ₃ | 6.77 | 5.47 | 6.26 | 3.98 | 4.86 | 5.01 | 7.27 | 1.73 | 7.84 | 4.60 | 5.12 | 7.19 | 0.88 |
| Cr ₂ O ₃ | 0.10 | 0.17 | B.d.l. | B.d.l. | B.d.l. | B.d.l. | B.d.l. | B.d.l. | 0.75 | 0.64 | B.d.l. | B.d.l. | B.d.l. |
| FeO* | 5.08 | 4.18 | 6.81 | 5.34 | 6.43 | 6.50 | 6.89 | 7.93 | 6.69 | 6.65 | 7.58 | 7.14 | 6.25 |
| MnO | 0.13 | 0.10 | 0.12 | 0.12 | 0.14 | 0.11 | 0.11 | 0.29 | 0.10 | 0.13 | 0.10 | 0.12 | 0.14 |
| MgO | 17.12 | 15.22 | 15.42 | 13.43 | 13.12 | 12.77 | 14.69 | 13.54 | 11.56 | 12.99 | 12.73 | 14.22 | 15.77 |
| CaO | 16.20 | 21.64 | 16.29 | 22.46 | 22.30 | 21.99 | 15.78 | 22.09 | 22.21 | 21.87 | 22.57 | 16.20 | 21.52 |
| Na ₂ O | 1.94 | 0.94 | 2.58 | 1.10 | 1.14 | 1.28 | 2.09 | 0.70 | 1.07 | 1.10 | 0.49 | 2.03 | 0.81 |
| Total | 101.0 | 101.0 | 100.6 | 99.9 | 100.6 | 100.8 | 100.5 | 98.3 | 100.7 | 100.0 | 99.3 | 99.81 | 99.79 |
| Wo, % | 36.75 | 46.90 | 40.67 | 47.17 | 49.89 | 49.51 | 37.55 | 47.96 | 52.00 | 49.03 | 49.89 | 38.87 | 44.96 |
| En | 54.05 | 45.91 | 47.19 | 46.61 | 40.84 | 40.00 | 48.63 | 40.91 | 37.65 | 40.52 | 39.16 | 47.48 | 45.86 |
| Fs | 9.20 | 7.19 | 12.71 | 5.64 | 9.28 | 10.50 | 13.81 | 11.13 | 10.35 | 10.46 | 10.96 | 13.65 | 9.18 |
| Mg# | 0.865 | 0.845 | 0.816 | 0.798 | 0.786 | 0.778 | 0.789 | 0.776 | 0.784 | 0.794 | 0.782 | 0.777 | 0.838 |

Note. Hereafter, B.d.l., below the detection limit of 0.1%.

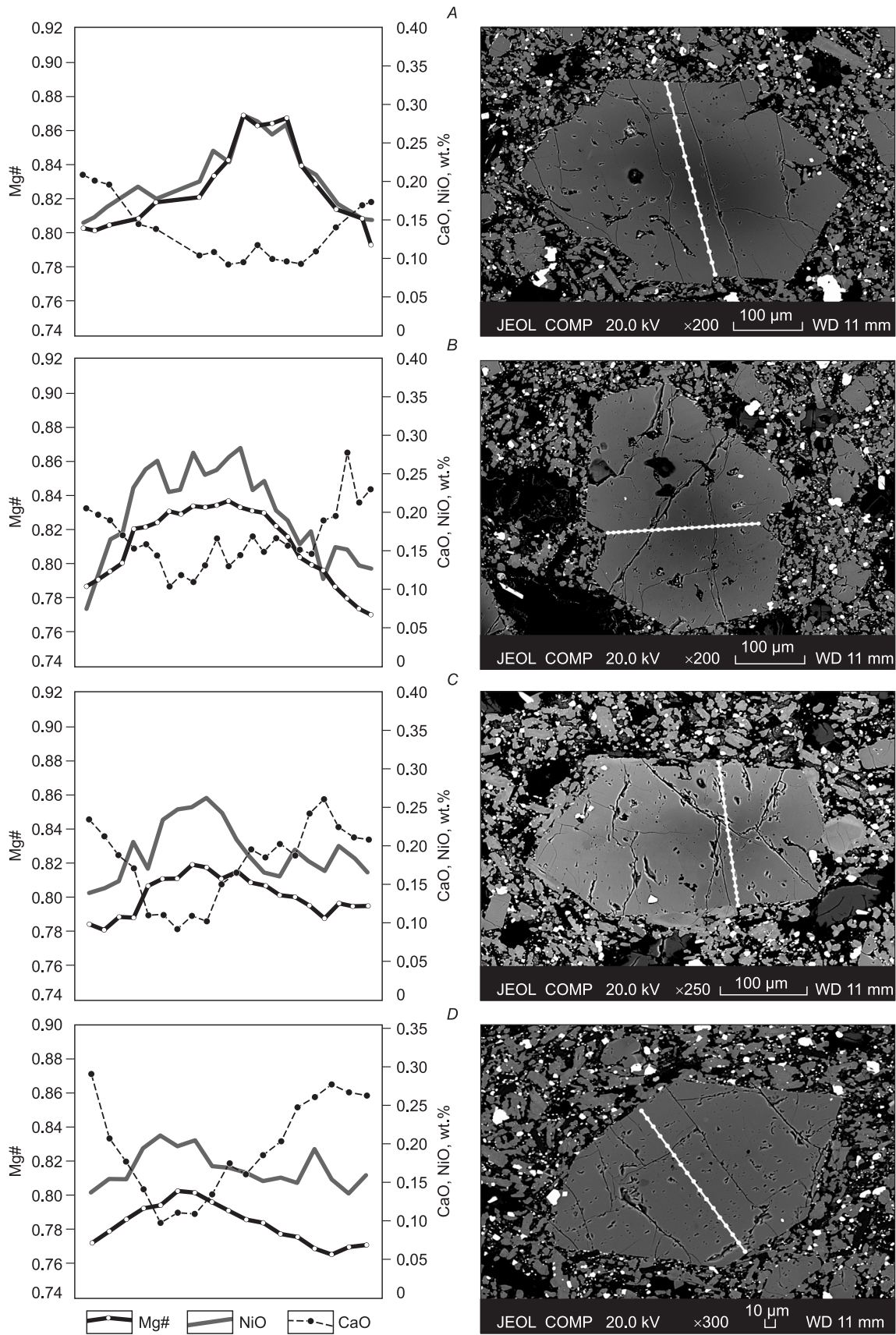


Fig. 5. CaO and NiO contents vs Mg# of olivine and BSE images of euhedral olivines (Superprobe JXA-8200 (JEOL Ltd, Japan) electron microprobe; accelerating voltage of 20 kV, beam current of 20 nA, and beam diameter of 1 μm). A, B14-26; B, B14-15; C, B14-15; D, B14-26.

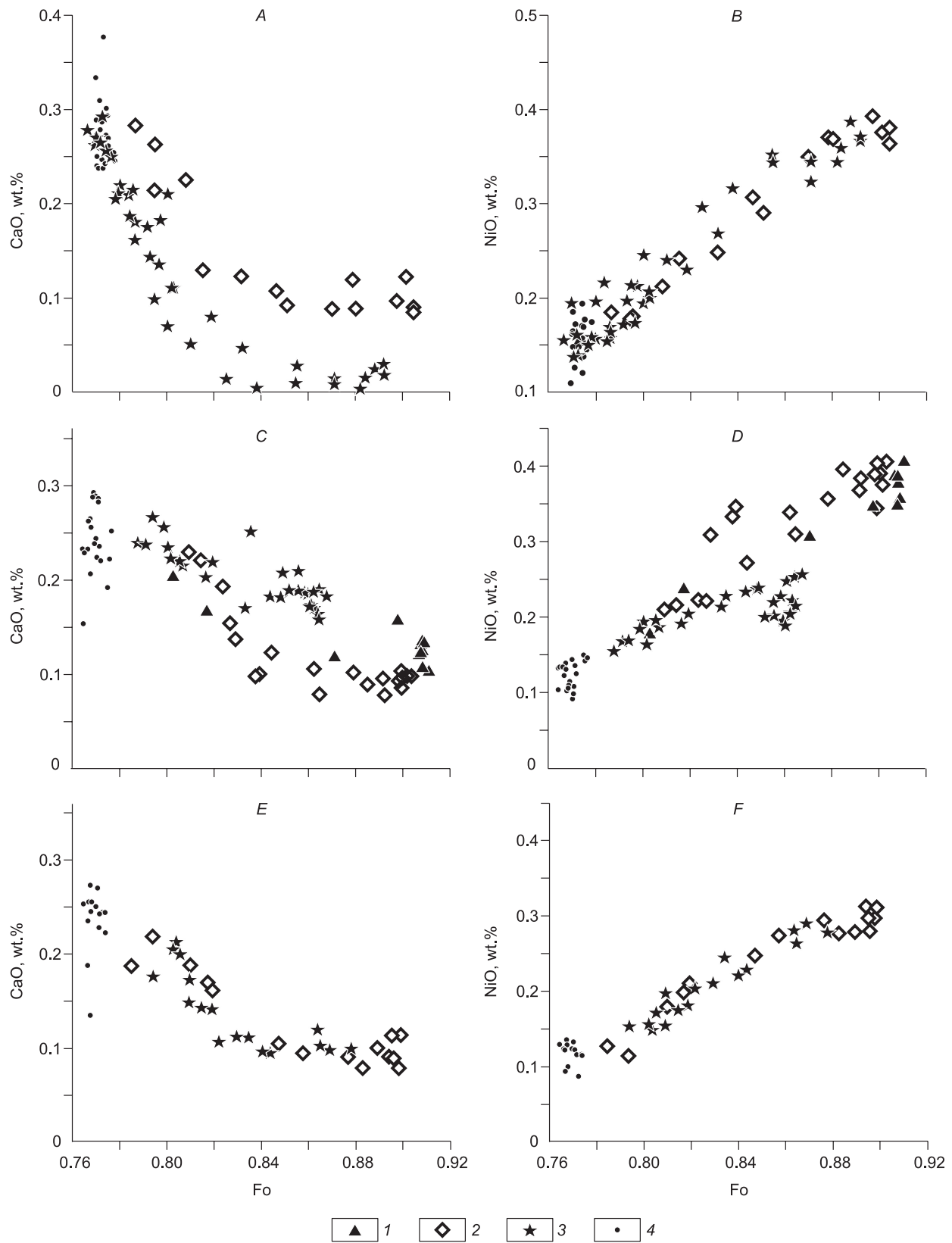


Fig. 6. CaO and NiO contents vs Fo of olivines of different generations. *A, B*, sample B26; *C, D*, sample B15; *E, F*, sample B11/2. 1, olivine from xenolith; 2, xenogenic olivine from peridotite (OI 1); 3, basaltic olivine (OI 2); 4, olivine from the groundmass (OI 3). Horizontal scale marks the content of forsterite molecule.

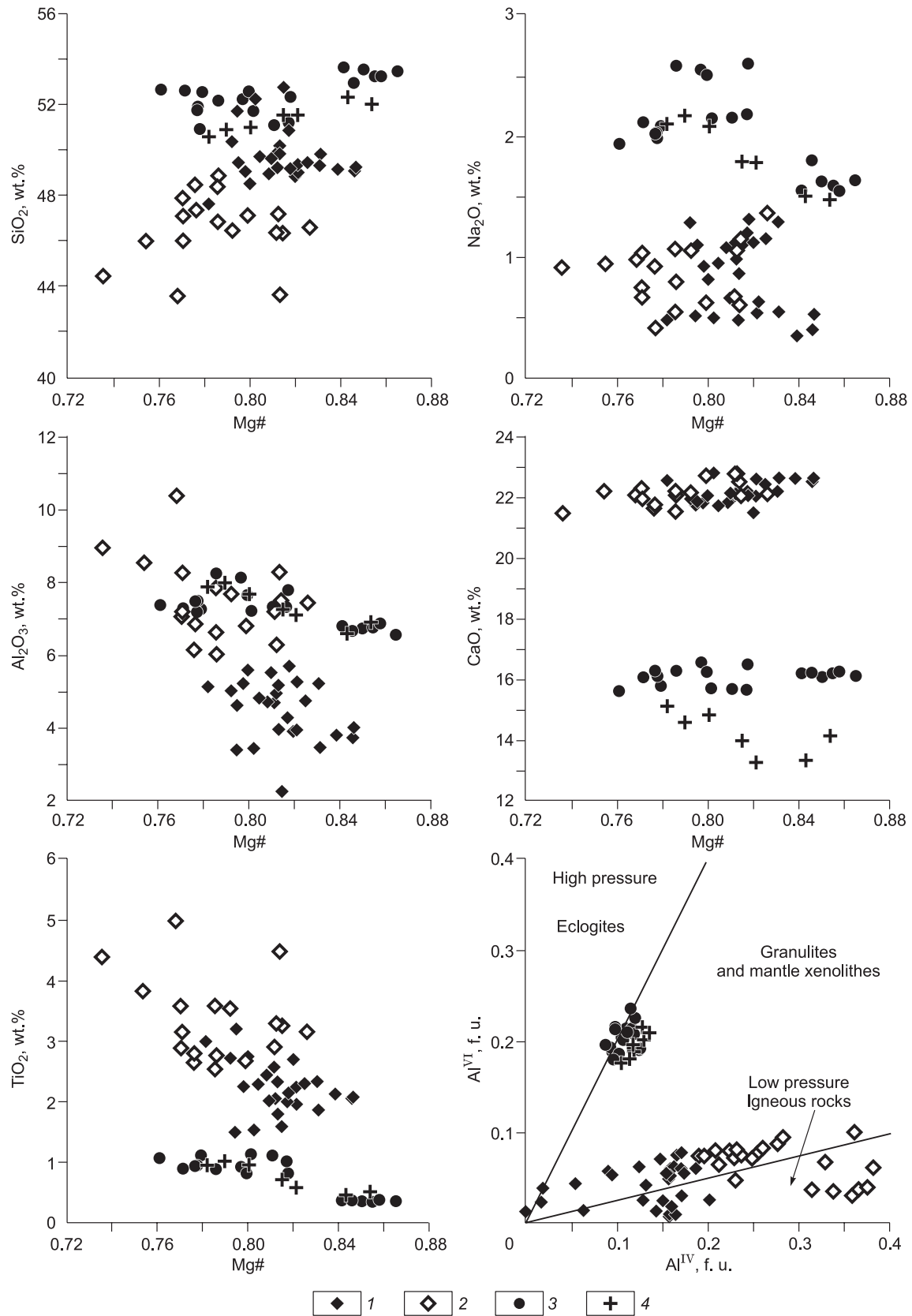


Fig. 8. Compositions of pyroxene phenocrysts and xenocrysts. 1, phenocryst cores, 2, phenocryst rims, 3, xenocrysts, 4, pyroxene xenocrysts from melanephelinitic lavas of the Khentei Ridge (Ashchepkov et al., 1996). The pressure/composition fields in the Al^{VI}-Al^{IV} diagram are given after Aoki and Shiba (1973).

Table 5. Results of representative analyses of oxide ore minerals

| Component | B11/3 | | | | | B15 | B26 | | | BB1 | B11/3 | | B15 | B11/3 | B26 |
|--------------------------------|----------|--------|--------|--------|--------|--------|--------|--------|--------|-------|-----------------|--------|-------|-------|-----|
| | Ilmenite | | | | | | | | | | Titanomagnetite | | | | |
| | | | | | | | | | | | Fine grains | | | | |
| TiO ₂ , wt.% | 52.91 | 52.20 | 50.86 | 52.20 | 52.46 | 42.78 | 50.51 | 50.53 | 51.26 | 9.31 | 8.96 | 10.35 | 9.97 | 6.21 | |
| Al ₂ O ₃ | 0.10 | 0.14 | 0.21 | B.d.l. | B.d.l. | 0.48 | 0.33 | 0.11 | 0.28 | 4.82 | 3.73 | 3.26 | 4.12 | 3.18 | |
| Cr ₂ O ₃ | 0.27 | 0.27 | 0.17 | 0.18 | 0.17 | 0.72 | 0.16 | 0.14 | B.d.l. | 2.08 | 1.78 | 3.93 | 2.26 | 1.88 | |
| V ₂ O ₃ | B.d.l. | B.d.l. | B.d.l. | 0.25 | B.d.l. | 0.24 | B.d.l. | 0.18 | B.d.l. | 0.11 | B.d.l. | B.d.l. | 0.10 | 0.10 | |
| Fe ₂ O ₃ | – | – | – | – | – | – | – | – | – | 50.00 | 52.48 | 50.90 | 49.87 | 54.49 | |
| FeO | 40.28 | 40.38 | 39.40 | 37.27 | 39.40 | 45.59 | 38.79 | 39.83 | 39.13 | 29.60 | 29.21 | 28.33 | 30.89 | 31.73 | |
| MnO | 0.59 | 0.56 | 0.34 | 0.70 | 0.34 | 0.61 | 0.34 | 0.66 | 0.70 | 0.12 | 0.13 | 0.44 | 0.18 | 0.16 | |
| NiO | B.d.l. | B.d.l. | B.d.l. | B.d.l. | B.d.l. | B.d.l. | B.d.l. | B.d.l. | B.d.l. | 0.25 | 0.26 | 0.22 | 0.24 | 0.28 | |
| MgO | 6.56 | 6.15 | 5.24 | 8.00 | 5.24 | 7.30 | 7.65 | 7.55 | 7.10 | 2.80 | 2.78 | 2.93 | 2.61 | 1.84 | |
| Total | 100.8 | 99.78 | 96.31 | 98.68 | 97.77 | 97.80 | 97.85 | 99.05 | 98.64 | 99.09 | 99.33 | 100.6 | 100.2 | 99.87 | |

| Component | B26 | | B11/3 | | | BB1 | | | B15 | | | | | | |
|--------------------------------|-----------------|-------|-----------------|--------|-------|--------|--------|-----------|--------|--------|--------|--------|--------|--------|--------|
| | Titanomagnetite | | Titanomagnetite | | | | | Cr-spinel | | | | | | | |
| | Large grains | | Large grains | | | | | core | | rim | | | | | |
| TiO ₂ , wt.% | 15.75 | 13.45 | 15.82 | 20.29 | 19.65 | 14.00 | 13.74 | 18.41 | 19.23 | 19.06 | 18.70 | 0.10 | 0.09 | 5.98 | 6.28 |
| Al ₂ O ₃ | 3.50 | 3.63 | 2.35 | 2.00 | 1.96 | 2.45 | 2.52 | 2.03 | 2.43 | 2.35 | 2.40 | 29.48 | 29.08 | 15.88 | 14.87 |
| Cr ₂ O ₃ | 0.75 | 1.37 | 0.81 | 1.07 | 1.11 | 0.80 | 0.71 | 0.59 | 0.93 | 0.96 | 0.99 | 34.51 | 34.95 | 20.20 | 20.14 |
| V ₂ O ₃ | B.d.l. | 0.19 | B.d.l. | B.d.l. | 0.15 | B.d.l. | B.d.l. | B.d.l. | B.d.l. | B.d.l. | B.d.l. | B.d.l. | B.d.l. | B.d.l. | B.d.l. |
| Fe ₂ O ₃ | 48.83 | 49.17 | 47.85 | 44.64 | 45.05 | 49.43 | 49.30 | 45.25 | 45.41 | 46.09 | 46.23 | 4.85 | 5.02 | 22.38 | 23.11 |
| FeO | 27.18 | 29.45 | 28.91 | 26.91 | 26.06 | 28.50 | 29.58 | 28.14 | 27.39 | 26.66 | 25.72 | 19.24 | 19.31 | 26.79 | 27.32 |
| MnO | 0.60 | 0.22 | 0.55 | 0.60 | 0.56 | 0.51 | 0.53 | 0.58 | 0.57 | 0.61 | 0.60 | 0.57 | 0.55 | 0.58 | 0.58 |
| NiO | 0.25 | 0.20 | 0.22 | 0.19 | 0.17 | 0.18 | 0.19 | 0.16 | 0.15 | 0.15 | 0.16 | 0.14 | 0.11 | 0.12 | 0.17 |
| MgO | 2.50 | 2.36 | 4.29 | 4.87 | 4.93 | 3.32 | 3.41 | 3.95 | 4.41 | 4.59 | 4.70 | 11.02 | 10.98 | 7.96 | 7.75 |
| Total | 99.36 | 100.0 | 100.8 | 100.8 | 99.58 | 99.19 | 99.98 | 99.11 | 100.5 | 100.4 | 99.50 | 99.94 | 100.1 | 99.99 | 100.3 |
| Mg# | – | – | – | – | – | – | – | – | – | – | – | 0.51 | 0.51 | 0.36 | 0.35 |
| Cr# | – | – | – | – | – | – | – | – | – | – | – | 0.44 | 0.45 | 0.46 | 0.48 |
| Fe# | – | – | – | – | – | – | – | – | – | – | – | 0.55 | 0.57 | 0.31 | 0.33 |

Note. The contents of Fe₂O₃ and FeO in Cr-spinel and titanomagnetite were calculated from their stoichiometric compositions.

phenocrysts, (2) fine laths in the groundmass, and (3) microlites in the finely crystallized matrix. Plagioclase from the phenocrysts contains up to 49% anorthite end-member. The laths are more sodic and have a composition Ab_{53–63}An_{35–45}Or_{1–2}. The interstitial plagioclase microlites have a felsic composition, Ab_{61–66}An_{11–25}Or_{10–22}. The interstices also contain nepheline and leucite (Table 4). The composition of leucite totally corresponds to the stoichiometric formula of the mineral. Nepheline contains up to 4 wt.% K₂O. Such contents of K are typical of nepheline (Samsonova, 1973; Ikor-skii, 1980).

Oxide ore minerals are represented by fine grains of ilmenite, titanomagnetite, and Cr-spinel. Their composition is given in Table 5.

Ilmenite is scattered in the groundmass. It is picroilmenite with MgO ≤ 8 wt.% and impurities of MnO (up to 0.70 wt.%), Cr₂O₃ (up to 0.70 wt.%), Al (tenths of wt.%), and V (tenths of wt.%) (Table 5). Such contents of impurities are specific to ilmenites of mafic rocks.

Titanomagnetite is present both as individual grains and in intergrowth with ilmenite (Fig. 9). Most of the fine titanomagnetite grains are homogeneous, whereas the larger

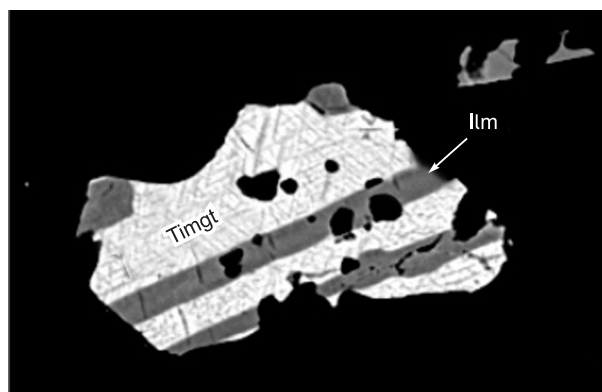


Fig. 9. BSE image of the oxide ore phase. Ilm, ilmenite, Timgt, disintegrated titanomagnetite, sample B11/3. Grain size is 40×50 μm.

grains have magnetite–ilmenite disintegration structures (Fig. 9). This might be due to the significantly lower content of TiO_2 in the fine grains (Table 5). The high content of TiO_2 in the large inclusions led to magnetite–ilmenite disintegration with decreasing temperature. The mineral contains many impurities (Table 5): It has high contents of Mg, Al, and Cr and medium contents of Ni and Mn relative to gabbro rocks. A similar mineral composition was observed in hawaiites and basanites of the Heven Plateau (Tsypukova et al., 2014). This leads us to the conclusion that such oxides are typical of alkali basalts.

Cr-spinel. The scarce Cr-spinel grains are zoned. Their cores are similar in composition (Table 5) to Cr-spinel from mantle xenoliths (Ashchepkov et al., 1996; Litasov and Taniguchi, 2002). These are, most likely, relics of garnet and spinel lherzolites. Similar Cr-spinel was found in basanites of the Heven Plateau (Tsypukova et al., 2014).

The present single sulfide grains are pyrrhotite with Fe = 78 wt.% and Ni \approx 3 wt.%.

MAJOR- AND TRACE-ELEMENT COMPOSITION OF THE ROCKS

The bulk major- and trace-element compositions of the samples are listed in Table 6.

The rocks are highly magnesian, $\text{MgO} = 11.81\text{--}14.77$ wt.%, and contain up to 15% normative nepheline. In the $(\text{Na}_2\text{O} + \text{K}_2\text{O})\text{--SiO}_2$ diagram, most of their composition points fall in the field of basanites (Fig. 10) (Le Bas et al., 1986). Three samples (B1, B04, and BB2) contain occasional olivine phenocrysts and thus can be considered aphyric. The aphyric and porphyritic basanites differ little in major-element composition. An increase in the number of phenocrysts in the rock is accompanied by an increase in the content of MgO and a decrease in the contents of other major components. An opposite pattern is observed in the aphyric varieties: a slight decrease in the contents of MgO (to

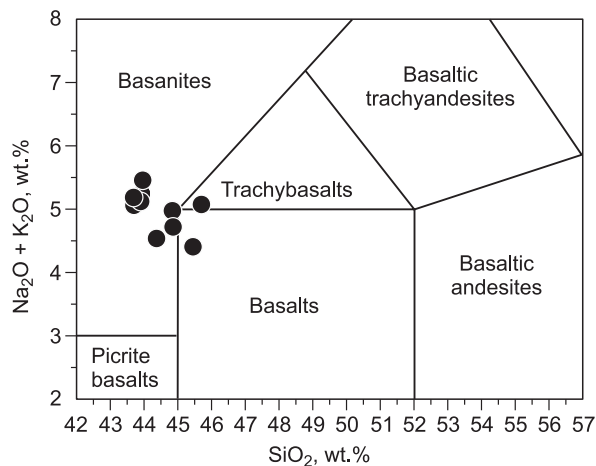


Fig. 10. $(\text{Na}_2\text{O} + \text{K}_2\text{O})\text{--SiO}_2$ composition diagram for volcanics of the Borozdin Bald Mountain (Le Bas et al., 1986).

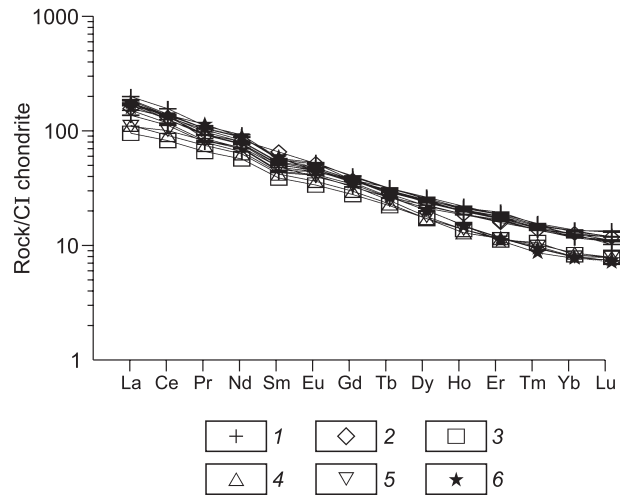


Fig. 11. REE patterns of volcanics from the Borozdin Bald Mountain and other volcanic areas of the South Baikal volcanic area. 1, volcanics of the Borozdin Bald Mountain; 2, OIB (Sun and McDonough, 1989); 3–5, alkali basalts of the SBVA, 3, Oka sector; 4, Tunka sector; 5, Hövsgöl sector (Yarmolyuk et al., 2003); 6, basanites of the Heven Plateau (Tsypukova et al., 2014).

2 wt.%), Cr, and Ni and a decrease in the content of Al_2O_3 . The rocks are rich in TiO_2 (>2 wt.%) and P_2O_5 (>0.5 wt.%). The studied volcanics belong to the Na–K series, because Na dominates over K. All samples are enriched in Cr (up to 1369 ppm), Ni (up to 686 ppm), REE, Nb, Sr, and Ba relative to the average oceanic-island melts (Naumov et al., 2016). We explain the high contents of Cr and Ni by a noticeable impurity of xenogenic minerals: high-Ni olivine and high-Cr Cr-spinel. Other trace elements are minor in the olivines, and their presence does not significantly change the geochemical features of the mineral. The REE pattern of basanites is identical to that of OIB (Fig. 11) (Sun and McDonough, 1989) and is also similar to the REE pattern of alkali basalts of the South Baikal volcanic province (Yarmolyuk et al., 2003; Tsypukova et al., 2014). One more spe-

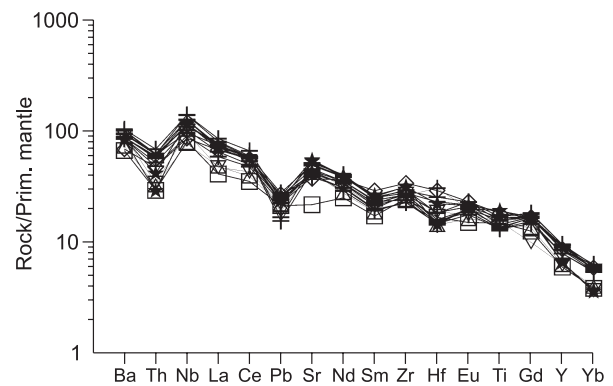


Fig. 12. Element patterns of volcanics from the Borozdin Bald Mountain and other volcanic areas of the South Baikal volcanic area. Designations follow Fig. 11.

Table 6. Chemical and trace-element (ppm) compositions of volcanics

| Component | B1 | B04 | B06 | B11/2 | B11/3 | B12 | B15 | B23 | B24 | BB1 | BB2 |
|----------------------------------|----------|-------|-------|-------|--------|----------|--------|----------|--------|-------|--------------|
| | Basanite | | | | Basalt | Basanite | Basalt | Basanite | | | Trachybasalt |
| SiO ₂ , wt.% | 43.93 | 43.70 | 43.90 | 44.84 | 45.45 | 44.84 | 43.69 | 44.86 | 44.37 | 43.96 | 45.70 |
| TiO ₂ | 3.02 | 2.56 | 2.76 | 2.42 | 2.00 | 2.12 | 2.95 | 2.35 | 2.11 | 2.57 | 2.76 |
| Al ₂ O ₃ | 12.51 | 12.09 | 11.98 | 11.86 | 11.47 | 11.86 | 11.88 | 11.62 | 11.55 | 12.04 | 12.47 |
| Fe ₂ O ₃ * | 11.73 | 11.80 | 11.39 | 11.28 | 12.87 | 12.25 | 11.58 | 11.02 | 12.62 | 11.47 | 11.07 |
| MnO | 0.19 | 0.19 | 0.19 | 0.19 | 0.18 | 0.19 | 0.18 | 0.19 | 0.19 | 0.18 | 0.18 |
| MgO | 12.27 | 12.66 | 13.56 | 14.02 | 14.49 | 14.02 | 13.29 | 14.77 | 14.63 | 12.84 | 11.81 |
| CaO | 9.94 | 9.89 | 9.83 | 9.32 | 9.61 | 9.32 | 9.96 | 9.35 | 9.51 | 9.81 | 9.90 |
| Na ₂ O | 3.57 | 3.56 | 3.72 | 3.54 | 3.15 | 3.54 | 3.68 | 3.31 | 3.21 | 3.79 | 3.72 |
| K ₂ O | 1.68 | 1.50 | 1.40 | 1.44 | 1.26 | 1.44 | 1.51 | 1.41 | 1.33 | 1.67 | 1.35 |
| P ₂ O ₅ | 0.68 | 0.62 | 0.76 | 0.61 | 0.50 | 0.61 | 0.62 | 0.54 | 0.65 | 0.65 | 0.53 |
| LOI | 0.34 | 0.45 | 0.26 | 0.24 | 0.17 | 0.24 | 0.22 | 0.27 | 0.16 | 0.25 | 0.24 |
| Total | 99.86 | 99.02 | 99.75 | 99.76 | 101.15 | 100.43 | 99.56 | 99.69 | 100.33 | 99.23 | 99.73 |
| Sc, ppm | 27 | 25 | 27 | 26 | 28 | 26 | 27 | 28 | 27 | 25 | 30 |
| V | 248 | 218 | 225 | 218 | 223 | 218 | 233 | 210 | 224 | 228 | 214 |
| Cr | 832 | 856 | 958 | 1022 | 1207 | 1369 | 1010 | 1314 | 979 | 729 | 707 |
| Co | 67 | 39 | 68 | 67 | 69 | 67 | 65 | 65 | 70 | 64 | 58 |
| Ni | 444 | 513 | 538 | 490 | 666 | 674 | 555 | 686 | 615 | 484 | 406 |
| Rb | 34 | 32 | 26 | 32 | 43 | 30 | 34 | 34 | 27 | 32 | 34 |
| Sr | 753 | 763 | 828 | 685 | 740 | 756 | 685 | 661 | 806 | 799 | 674 |
| Y | 32 | 32 | 32 | 29 | 21 | 27 | 28 | 27 | 30 | 29 | 29 |
| Zr | 243 | 227 | 238 | 210 | 187 | 210 | 220 | 187 | 197 | 217 | 219 |
| Nb | 78 | 61 | 78 | 65 | 50 | 65 | 70 | 57 | 64 | 71 | 70 |
| Ba | 491 | 452 | 441 | 412 | 432 | 443 | 419 | 404 | 441 | 479 | 515 |
| La | 44 | 43 | 47 | 39 | 41 | 32 | 41 | 36 | 41 | 41 | 39 |
| Ce | 85 | 83 | 95 | 77 | 68 | 76 | 81 | 77 | 82 | 77 | 84 |
| Pr | 10.0 | 9.90 | 10.50 | 8.70 | 7.50 | 8.70 | 8.80 | 7.80 | 9.30 | 8.80 | 9.10 |
| Nd | 41 | 41 | 43 | 36 | 31 | 36 | 38 | 32 | 37 | 35 | 33 |
| Sm | 8.60 | 8.70 | 8.80 | 7.30 | 6.60 | 7.30 | 8.20 | 6.70 | 8.00 | 7.80 | 6.90 |
| Eu | 2.99 | 2.81 | 2.99 | 2.57 | 2.29 | 2.57 | 2.71 | 2.33 | 2.62 | 2.63 | 2.46 |
| Gd | 8.30 | 7.80 | 8.30 | 7.70 | 6.70 | 7.70 | 8.00 | 7.30 | 7.50 | 7.90 | 8.10 |
| Tb | 0.99 | 0.99 | 1.06 | 0.96 | 0.98 | 1.08 | 1.00 | 0.88 | 1.11 | 0.98 | 0.98 |
| Dy | 6.70 | 6.40 | 6.50 | 6.20 | 5.40 | 6.20 | 6.00 | 5.70 | 6.30 | 6.30 | 6.10 |
| Ho | 1.24 | 1.16 | 1.19 | 1.13 | 1.04 | 1.13 | 1.12 | 1.06 | 1.20 | 1.11 | 1.13 |
| Er | 3.06 | 2.97 | 3.08 | 2.89 | 2.70 | 1.89 | 2.80 | 2.25 | 3.23 | 2.85 | 2.97 |
| Tm | 0.38 | 0.36 | 0.38 | 0.37 | 0.35 | 0.37 | 0.34 | 0.35 | 0.39 | 0.35 | 0.38 |
| Yb | 2.28 | 2.04 | 2.09 | 2.14 | 2.32 | 1.98 | 2.03 | 2.01 | 2.23 | 2.12 | 2.28 |
| Lu | 0.30 | 0.27 | 0.30 | 0.28 | 0.27 | 0.28 | 0.28 | 0.28 | 0.30 | 0.26 | 0.34 |
| Ta | 4.38 | 3.61 | 4.30 | 3.59 | 2.91 | 3.59 | 4.00 | 3.21 | 3.48 | 3.75 | 4.01 |
| Hf | 4.88 | 6.17 | 6.81 | 3.93 | 3.93 | 3.93 | 4.95 | 4.17 | 3.85 | 4.06 | 4.27 |
| Pb | 3.31 | 1.99 | 2.86 | 2.84 | 2.70 | 2.84 | 1.84 | 2.86 | 3.09 | 2.29 | 2.65 |
| Th | 5.82 | 5.24 | 5.21 | 4.88 | 4.29 | 5.10 | 4.79 | 4.41 | 5.30 | 5.07 | 5.30 |
| U | 1.52 | 1.38 | 1.52 | 1.33 | 1.13 | 1.32 | 1.27 | 1.15 | 1.36 | 1.38 | 1.29 |

Note. Analyzed by V.I. Lozhkin, N.N. Pakhomova, and A.L. Finkel'shtein.
Fe₂O₃* is total iron.

cific geochemical feature is a high degree of REE fractionation ($La/Yb = 16–20$; $Dy/Yb = 2.7–3.1$). The indicator ratios of trace elements in the volcanics are also close to those in OIB ($Ba/Nb = 6.5–9.5$; $Nb/Zr = 0.29–0.32$). Basaltoids of the Borozdin Bald Mountain are enriched in HFSE

relative to LILE and LREE and have low Rb/Sr and high U/Pb and Th/Pb ratios.

The spidergram of the studied rocks (Fig. 12) shows their identity to alkali basalts of the South Baikal volcanic province.

Table 7. Isotope characteristics of basaltoids

| Sample | $^{87}\text{Rb}/^{86}\text{Sr}$ | $(^{87}\text{Sr}/^{86}\text{Sr})_{\text{meas}}$ | $\pm 2\text{SE}$ | ϵ_{Sr} | $^{147}\text{Sm}/^{144}\text{Nd}$ | $(^{143}\text{Nd}/^{144}\text{Nd})_{\text{meas}}$ | $\pm 2\text{SE}$ | ϵ_{Nd} | $^{206}\text{Pb}/^{204}\text{Pb}$ | $\pm 2\text{SE}$ | $^{207}\text{Pb}/^{204}\text{Pb}$ | $\pm 2\text{SE}$ | $^{208}\text{Pb}/^{204}\text{Pb}$ | $\pm 2\text{SE}$ |
|--------|---------------------------------|---|------------------|------------------------|-----------------------------------|---|------------------|------------------------|-----------------------------------|------------------|-----------------------------------|------------------|-----------------------------------|------------------|
| BB1 | 0.1391 | 0.70385 | 3 | -9.2 | 0.1307 | 0.512948 | 22 | 6.0 | 18.8412 | 18 | 15.5410 | 14 | 38.8903 | 38 |
| B11/2 | 0.1670 | 0.70392 | 2 | -8.2 | 0.1311 | 0.512888 | 8 | 4.9 | 18.8142 | 13 | 15.5430 | 12 | 38.8628 | 31 |
| B15 | 0.1300 | 0.70386 | 1 | -9.1 | 0.1319 | 0.512919 | 10 | 5.5 | 18.6751 | 12 | 15.5325 | 10 | 38.6828 | 29 |
| B26 | 0.0998 | 0.70384 | 4 | -9.4 | 0.1297 | 0.512925 | 6 | 5.6 | 18.4971 | 20 | 15.5281 | 17 | 38.4961 | 45 |

ISOTOPE CHARACTERISTICS OF BASALTOIDS

According to modern concepts, OIB might form from HIMU, EM I, and EM II reservoirs (Weaver, 1991). To elucidate the nature of the isotope sources of basaltoids of the Borozdin Bald Mountain, we studied the Sr, Nd, and Pb isotope compositions of the rocks. The results of the analyses are listed in Table 7. The isotope characteristics of Cenozoic basaltoids of the South Baikal (SBVA) and South Hangayn (SHVA) volcanic areas are reported elsewhere (Rasskazov et al., 2002; Barry et al., 2003; Yarmolyuk et al., 2003; Savatenkov et al., 2010; Tsyukova et al., 2014). The studies showed that the variations in the Sr, Nd, and Pb isotope compositions in these basaltoids are determined mostly by the interaction between depleted (DM and/or PREMA) and enriched (EM I) mantle sources. The basaltoids of the Boro-

zdin Bald Mountain differ slightly in isotope characteristics. Their Sr–Nd isotope composition (Fig. 13) indicates that the rocks formed from a moderately depleted PREMA-type source, because they are stronger depleted in Nd ($\epsilon_{\text{Nd}} = 4.9$ – 6.1) and Sr ($^{87}\text{Sr}/^{86}\text{Sr} = 0.7038$ – 0.7039) than the SBVA and SHVA basaltoids ($\epsilon_{\text{Nd}} \leq 4$ and $^{87}\text{Sr}/^{86}\text{Sr} \geq 0.7041$). At the same time, the studied basaltoids have a more radiogenic Pb isotope composition than the SBVA and SHVA ones and the average MORB and PREMA, as seen from the $^{207}\text{Pb}/^{204}\text{Pb}$ – $^{206}\text{Pb}/^{204}\text{Pb}$ (Fig. 14A) and $^{208}\text{Pb}/^{204}\text{Pb}$ – $^{206}\text{Pb}/^{204}\text{Pb}$ (Fig. 14B) diagrams. The composition points of basaltoids from the Borozdin Bald Mountain, SBVA, and SHVA form common trends ending with the most radiogenic compositions. Additional radiogenic Pb isotopes might come from EM II and HIMU. In the ϵ_{Nd} – $^{206}\text{Pb}/^{204}\text{Pb}$ diagram (Fig. 15A), the composition points of the Borozdin basaltoids form a

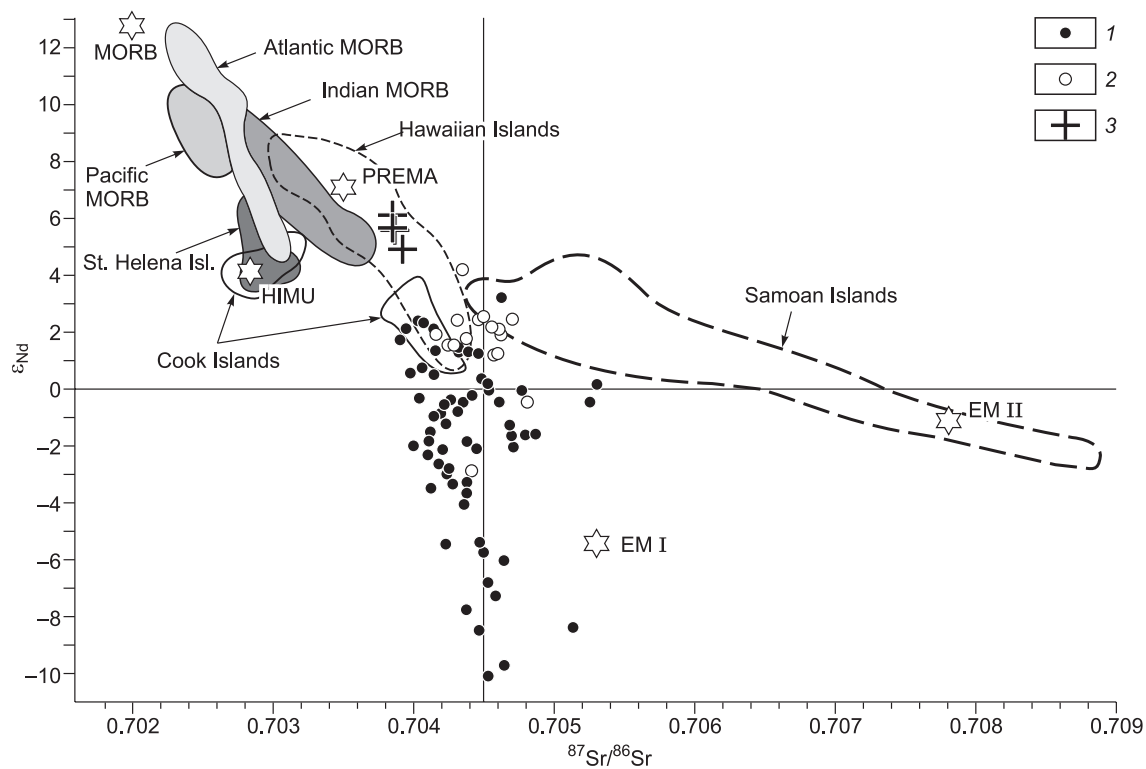


Fig. 13. ϵ_{Nd} – $^{87}\text{Sr}/^{86}\text{Sr}$ diagram for Neogene basaltoids: 1, SBVA (Rasskazov et al., 2002; Yarmolyuk et al., 2003; Tsyukova et al., 2014); 2, SHVA (Barry et al., 2003; Savatenkov et al., 2010), 3, Borozdin Bald Mountain. Fields mark the compositions of EM I, EM II, and HIMU (Armienti and Gasperini, 2007; Jackson and Dasgupta, 2008), PREMA (Zindler and Hart, 1986), Atlantic MORB (Paulick et al., 2010; Skolotnev, 2014), Pacific MORB (Hamelin et al., 2011), Indian MORB (Mahoney et al., 2002), Hawaiian OIB (Stracke, 2012), St. Helena OIB (Chaffey et al., 1989), Cook OIB (Palacz and Saunders, 1986), and Samoa OIB (Palacz and Saunders, 1986; Workman et al., 2004).

compact cluster separated from the points of the SBVA and SHVA basalts and shifted relative to PREMA toward more radiogenic $^{206}\text{Pb}/^{204}\text{Pb}$ values. As in the diagrams of Pb isotope evolution, this shift is minor; therefore, it is impossible to determine the source of radiogenic Pb reliably. To solve this problem, we can estimate varia-

tions in the isotope compositions of the Borozdin basalts from the $^{87}\text{Sr}/^{86}\text{Sr}$ – $^{206}\text{Pb}/^{204}\text{Pb}$ diagram (Fig. 15B), where their composition points form a clear trend from PREMA to HIMU. This trend shows a constant depleted isotope composition of Sr and an increase in the content of radiogenic Pb isotope.

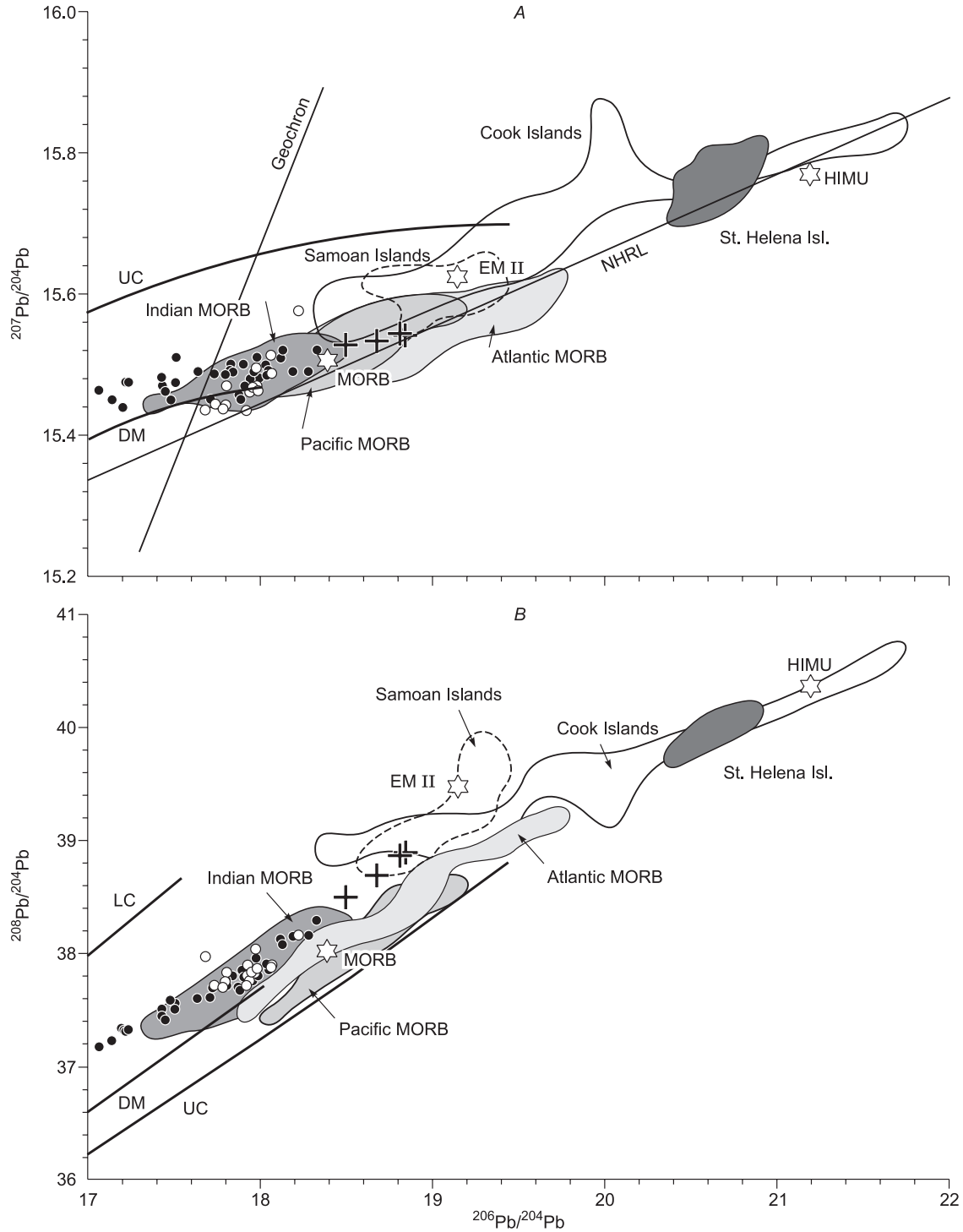


Fig. 14. $^{207}\text{Pb}/^{204}\text{Pb}$ – $^{206}\text{Pb}/^{204}\text{Pb}$ (A) and $^{208}\text{Pb}/^{204}\text{Pb}$ – $^{206}\text{Pb}/^{204}\text{Pb}$ (B) diagrams for Neogene basalts. Isotope trends of Pb in the upper crust (UC), lower crust (LC), and depleted mantle (DM) (Zartman and Doe, 1981) are shown. Other designations follow Fig. 13.

Thus, the Sr–Nd–Pb isotope data show that PREMA was the main mantle source of substance for the Borozdin basaltoids, whereas HIMU was a subordinate source, in contrast to the SBVA and SHVA basaltoids, whose isotope composition was determined by mixing of PREMA and EM I.

MANTLE SOURCES AND COMPOSITION OF THE PARENTAL MELT

Note that even the minor amount of xenogenic olivine (especially high-Mg one) and augite in the basanites distorted their major-element composition, namely, led to their

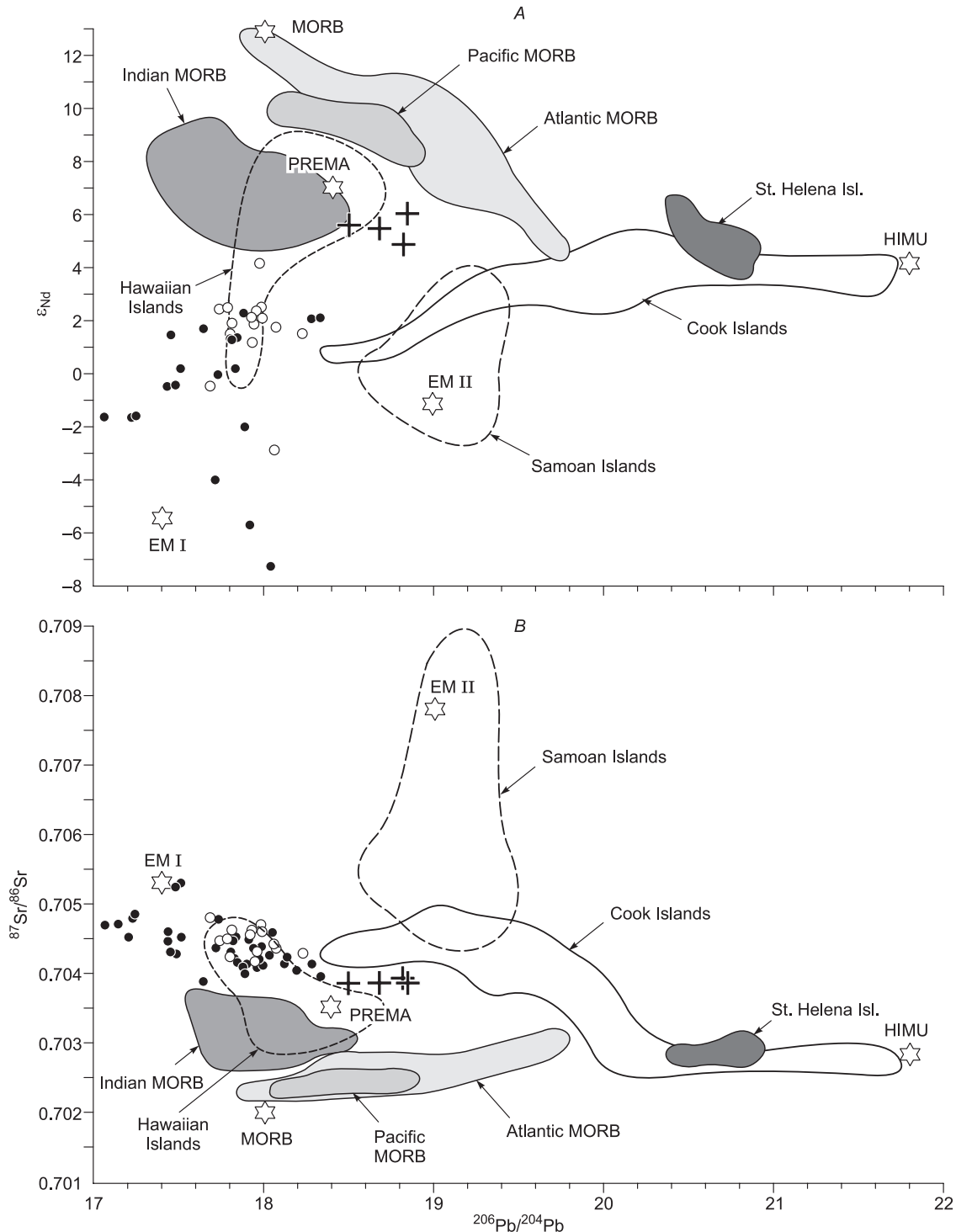


Fig. 15. ϵ_{Nd} - $^{206}Pb/^{204}Pb$ (A) and $^{87}Sr/^{86}Sr$ - $^{206}Pb/^{204}Pb$ (B) diagrams for Neogene basaltoids. Other designations follow Fig. 13.

Table 8. Calculated composition of the parental melt, wt.%

| Sample | SiO ₂ | TiO ₂ | Al ₂ O ₃ | Fe ₂ O ₃ | FeO | MnO | MgO | CaO | Na ₂ O | K ₂ O | P ₂ O ₅ | Total |
|--------|------------------|------------------|--------------------------------|--------------------------------|-------|------|------|-------|-------------------|------------------|-------------------------------|-------|
| B1 | 44.99 | 3.37 | 13.98 | 1.67 | 9.41 | 0.20 | 8.70 | 11.10 | 3.96 | 1.87 | 0.75 | 100 |
| B04 | 45.14 | 3.27 | 12.46 | 1.81 | 10.29 | 0.19 | 9.61 | 10.79 | 3.88 | 1.83 | 0.73 | 100 |
| BB1 | 45.38 | 2.95 | 13.77 | 1.67 | 9.13 | 0.20 | 8.69 | 11.22 | 4.32 | 1.86 | 0.72 | 100 |
| B23 | 46.37 | 2.80 | 14.09 | 1.55 | 8.70 | 0.20 | 8.30 | 11.39 | 4.10 | 1.80 | 0.70 | 100 |
| B24 | 45.81 | 2.40 | 13.18 | 1.65 | 10.20 | 0.22 | 9.85 | 10.80 | 3.65 | 1.50 | 0.74 | 100 |

high Mg# values. This, however, did not significantly influence the distribution of trace elements.

The composition of the parental melt (Herzberg, 2006) can be calculated from the composition of aphyric basalts. Parental melt implies the melt in equilibrium with the most magnesian olivine phenocryst found in the examined basalts. The compositions of the parental melt of the Borozdin basanites are in equilibrium with olivine with Mg# = 0.86. To obtain the parental melt, we removed olivine with Mg# = 0.91 from five rock samples step by step until equilibrium between the melt and olivine with Mg# = 0.86 was reached. The removal of olivine and estimation of the melt–olivine equilibrium were made using special appendices (Putirka, 2008; Danyushevsky and Plechov, 2011). The calculated composition of the parental melt equilibrated with olivine with Mg# = 0.86 is given in Table 8. This melt has a nepheline-normative composition and medium contents of MgO and CaO. The temperatures and pressures of the olivine–melt and diopside–melt equilibria in the cores of olivine grains from basanites were calculated following the technique described by Putirka (2008). The calculation yielded the following crystallization temperatures and pressures of the equilibria between Fo_{0.86} and basanitic melt: 1379–1293 °C and 1.15–1.06 GPa. Thus, the parental melt began to form at a temperature no lower than 1370 °C and a pressure no lower than 1.15 GPa. Diopside was the next to crystallize. Following the same technique (Putirka, 2008), we estimated the temperature and pressure of crystallization of the cores of diopside phenocrysts (Wo = 44.96, En = 45.86, Fs = 9.18%): 1174–1122 °C and 0.94–0.926 GPa. The difference in the *P–T* parameters of olivine and diopside suggests a rapid ascent of the melt. The same is evidenced by the zoned structure of both olivine and pyroxene phenocrysts. If the melt stayed in the intermediate chambers for a long time, then the crystals would be completely homogenized.

Analysis of experimental data on melting of peridotites and of results of petrological studies showed (Herzberg, 2006, 2011) that primary melts resulting from melting of peridotites have higher contents of CaO than the products of melting of a pyroxenite source. Calculation using the PRIMELT3 software (Herzberg and Asimow, 2015) yielded a low content of CaO in the parental melt of the Borozdin basaltoids, which suggests a pyroxenite source of the melt. This is consistent with the low content of CaO in the most

magnesian olivine phenocrysts in the Borozdin basanites. As shown earlier (Sobolev et al., 2005, 2007), olivine phenocrysts from basalts formed from pyroxenites have lower contents of CaO and MnO and higher contents of NiO than olivines from effusive rocks formed from a peridotite source.

Herzberg (2011) regards olivine pyroxenites (Ol + Cpx + Grt) as a mantle source for nepheline-normative OIB. They might be a cumulative part of recycled oceanic crust or the result of solid-phase reactions between eclogites and peridotites in the lower mantle (Herzberg, 2011). Partial melting of olivine pyroxenites might yield melts with characteristics demonstrated by the Borozdin basanites (low SiO₂ and CaO contents and a high MgO content). The presence of olivine in the restite accounts for the “peridotite” contents of NiO in the olivine phenocrysts.

The above hypothesis is confirmed by the localization of the composition points of the studied volcanics and xenogenic olivines in the same curve in the MgO–Ni diagram (Fig. 16), which was earlier assumed by Sobolev et al. (2005, 2007). We calculated the temperature and pressure of crystallization of xenogenic augite, following the technique of Putirka (2008): 1173–1181 °C and 1.03 GPa. Thus, the basanitic melt trapped these phases, which is confirmed by the *P–T* conditions of formation of the parental melt (see above).

Some researchers associate the volcanism in this region with the mantle diapir activity (Ashchepkov et al., 1996; Litasov and Taniguchi, 2002). We believe that the studied basaltoid melts resulted from the ascending mantle plume, like the rock melts of the Heven Plateau (Tsybukova et al., 2014).

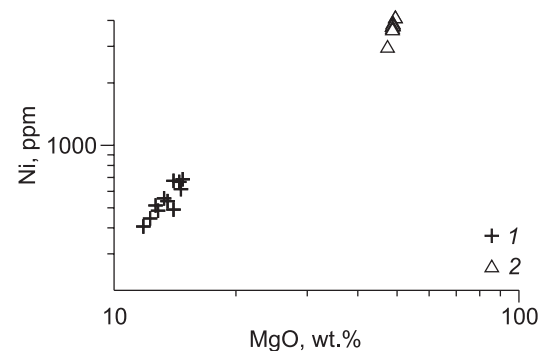


Fig. 16. Ni–MgO correlation diagram. 1, basanites, 2, xenogenic olivines.

CONCLUSIONS

We have estimated the P – T conditions of formation of basaltoid melts: $P = 1.15$ – 1.06 GPa and $T = 1379$ – 1293 °C. Olivine pyroxenites (Ol + Cpx + Grt) are assumed to be a mantle source for nepheline-normative basanitic melts. During ascent, the melt trapped mantle xenoliths, which were disintegrated into olivine and augite xenocrysts.

The volcanic area of southern Transbaikalia (Khentei Ridge) resulted, most likely, from the mantle plume impact on the lithosphere. The age of this area is estimated at 3.51 Ma. PREMA was the main mantle source for these volcanics, and the contribution of HIMU was strongly subordinate. In geochemical features the studied volcanics correspond to mafic rocks of oceanic islands. They are similar in composition to alkali basalts of the South Baikal volcanic area.

We thank the analysts of the Institute of Geochemistry, Irkutsk, for help.

The research was carried out on state assignment under project IX.129.1.5 No. 0350-2016-0030 AAAA-A17-117041910032-1 with a financial support by grant 17-05-00928 from the Russian Foundation for Basic Research.

REFERENCES

- Afonin, V.P., Gunicheva, T.N., Piskunova, L.F., 1984. X-Ray Fluorescence Analysis [in Russian]. Nauka, Novosibirsk.
- Al'mukhamedov, A.I., Juteau, T., Matveenkov, V.V., Eissen, J.-P., Kashintsev, G.L., 1983. Geochemistry of Red Sea low-K tholeiites. *Geokhimiya*, No. 9, 1289–1303.
- Al'mukhamedov, A.I., Kashintsev, G.L., Matveenkov, V.V., 1985. Evolution of Basaltic Volcanism in the Red Sea Region [in Russian]. Nauka, Novosibirsk.
- Aoki, K., Shiba, I., 1973. Pyroxenes from lherzolite inclusions of Itinome-gata, Japan. *Lithos* 6, 41–51.
- Armienti, P., Gasperini, D., 2007. Do we really need mantle components to define mantle composition? *J. Petrol.* 48 (4), 693–709.
- Ashchepkov, I.V., Litasov, Yu.D., Litasov, K.D., 1996. Xenoliths of garnet lherzolites from metanephelinites, the Khentei Ridge (Southern Transbaikalia): evidence for the uplift of mantle diapir. *Geologiya i Geofizika* (Russian Geology and Geophysics) 37 (1), 130–147 (121–137).
- Barry, T.L., Saunders, A.D., Kempton, P.D., Windley, B.F., Pringle, M.S., Dorjnamjaa, D., Saandar, S., 2003. Petrogenesis of Cenozoic basalts from Mongolia: evidence for the role of asthenospheric versus metasomatized lithospheric mantle sources. *J. Petrol.* 44 (1), 55–91.
- Buikin, A.I., Trieloff, M., Koroshantseva, E., Hopp, J., Kaliwoda, M., Meyer, H.-P., Altherr, R., 2010. Distribution of mantle and atmospheric argon in mantle xenoliths from the Western Arabian Peninsula: constraints on timing and composition of metasomatizing agents in the lithospheric mantle. *J. Petrol.* 51 (12), 2547–2570.
- Buslov, M.M., 2012. Geodynamic nature of the Baikal Rift Zone and its sedimentary filling in the Cretaceous–Cenozoic: the effect of the far-range impact of the Mongolo–Okhotsk and Indo–Eurasian collisions. *Russian Geology and Geophysics* (Geologiya i Geofizika) 53 (9), 955–962 (1245–1255).
- Chaffey, D.J., Cliff, R.A., Wilson, B.M., 1989. Characterization of the St. Helena magma source, in: Saunders, A.D., Norry, M.J. (Eds.), *Magmatism in the Ocean Basins*. Geol. Soc. London Spec. Publ. 42, 257–300.
- Costa, F., Dungan, M., 2005. Short time scales of magmatic assimilation from diffusion modeling of multiple elements in olivine. *Geology* 33 (10), 837–840.
- Danyushevsky, L.V., Plechov, P.Yu., 2011. Petrolog3: Integrated software for modeling crystallization processes. *Geochem. Geophys. Geosyst.* 12 (7), doi:10.1029/2011GC003516.
- Donaldson, C.H., 1985. The rates of dissolution of olivine, plagioclase and quartz in a basalt melt. *Mineral. Mag.* 49 (354), 683–693.
- Finkel'shtein, A.L., Gunicheva, T.N., Afonin, V.P., 1984. The accounting of matrix effects by the alpha correction method during an X-ray fluorescence analysis. *Zhurnal Analiticheskoi Khimii* 39 (3), 397–404.
- Hamilin, C., Dosso, L., Hannan, B.B., Moreira, M., Kositsky, A.P., Thomas, M.Y., 2011. Geochemical portrait of the Pacific Ridge: New isotopic data and statistical techniques. *Earth Planet. Sci. Lett.* 302 (1–2), 154–162.
- Herzberg, C., 2006. Petrology and thermal structure of the Hawaiian plume from Mauna Kea volcano. *Nature* 444 (7119), 605–609.
- Herzberg, C., 2011. Identification of source lithology in the Hawaiian and Canary Islands: Implications for origins. *J. Petrol.* 52 (1), 113–146.
- Herzberg, C., Asimow, P.D., 2015. PRIMELT3 MEGA. XLSM software for primary magma calculation: Peridotite primary magma MgO contents from the liquidus to the solidus. *Geochem. Geophys. Geosyst.* 16 (2), 563–578.
- Ikorskii, S.V., 1980. Typomorphic compositional and structural features of nepheline. *Geokhimiya*, No. 5, 608–710.
- Ivanov, A.V., Meffre, S., Thompson, J., Corfu, F., Kamenetsky, V.S., Kamenetsky, M.B., Demonerova, E.I., 2017. Timing and genesis of the Karoo–Ferrar large igneous province: New high-precision U–Pb data for Tasmania confirm short duration of the major magmatic pulse. *Chem. Geol.* 455, 32–43.
- Ivanov, A.V., Mukasa, S.B., Kamenetsky, V.S., Ackerson, M., Demonerova, E.I., Pokrovsky, B.G., Vladykin, N.V., Kolesnichenko, M.V., Litasov, K.D., Zedgenizov, D.A., 2018. Volatile concentrations in olivine-hosted melt inclusions from meimechite and melanephelinite lavas of the Siberian Traps Large Igneous Province: Evidence for flux-related high-Ti, high-Mg magmatism. *Chem. Geol.* 483, 442–462.
- Jackson, M.G., Dasgupta, R., 2008. Composition of HIMU, EM1, and EM2 from global trends between radiogenic isotopes and major elements in ocean island basalts. *Earth Planet. Sci. Lett.* 276 (1), 175–186.
- Kiselev, A.I., Medvedev, M.E., Golovko, G.A., 1979. Volcanism in the Baikal Rift Zone and Problems of Deep Magma Formation [in Russian]. Nauka, Novosibirsk.
- Kostyakov, N.P., Krasnov, V.P., Ufimtsev, G.F., Yankovskii, V.M., 1969. Cenozoic basalts in the south of central Transbaikalia. *Izvestiya Zabaikal'skogo Geograficheskogo Obshchestva SSSR* 5 (1), 11–17.
- Kovalenko, V.I., Yarmolyuk, V.V., Kovach, V.P., Budnikov, S.V., Zhuravlev, D.E., Kozakov, I.K., Kotov, A.B., Rytsk, E.Yu., Sal'nikova, E.B., 1999. Crust-forming processes and structure of the mantle crust during the formation of the Central Asian Orogenic Belt: Sm–Nd isotope data. *Geotektonika*, No. 3, 21–41.
- Kovalenko, V.I., Yarmolyuk, V.V., Bogatkov, O.A., 2009. Geodynamic setting of recent volcanism in North Eurasia. *Geotectonics* 43 (5), 337–357.
- Laverov, N.P. (Ed.), 2008. Recent volcanism in northern Eurasia: regularities of evolution, volcanic hazard, and relationship with deep processes and environmental and climate changes, in: *Environmental and Climate Changes: Natural and Associated Man-Induced Disasters* [in Russian]. IGEM RAN, IFZ RAN, Moscow, Vol. 2.
- Le Bas, M.J., Le Maitre, R.W., Streckeisen, A., Zanettin, B.A., 1986. A chemical classification of volcanic rocks based on the total alkali-silica diagram. *J. Petrol.* 27 (3), 745–750.
- Liang, Y., 2000. Dissolution in molten silicates: Effects of solid solution. *Geochim. Cosmochim. Acta* 64 (9), 1617–1627.

- Litasov, K., Taniguchi, H., 2002. Mantle Evolution beneath the Baikal Rift. Tohoku University, Sendai. CNEAS Monograph Series, Vol. 5.
- Logachev, N.A., 2003. History and geodynamics of the Baikal rift. *Geologiya i Geofizika (Russian Geology and Geophysics)* 44 (5), 391–406 (373–387).
- Mahoney, J.J., Graham, D.W., Christie, D.M., Johnson, K.T.M., Hall, L.S., Vonderhaar, D.L., 2002. Between a hotspot and a cold spot: isotopic variation in the Southeast Indian Ridge asthenosphere, 86 °E–118 °E. *J. Petrol.* 43 (7), 1155–1176.
- Mysovskaya, I.N., Smirnova, E.V., Lozhkin, V.I., Pakhomova, N.N., 2009. New data on ICP MS determination of trace and scattered elements in geologic standard samples. *Zavodskaya Laboratoriya. Diagnostika Materialov*, No. 10, 60–66.
- Naumov, V.B., Dorofeeva, V.A., Girnis, A.V., 2016. Volatile and trace elements in alkaline and subalkaline melts of ocean islands: evidence from inclusions in minerals and quenched glasses of rocks. *Geochem. Int.* 54 (6), 543–558.
- Palacz, Z.A., Saunders, A.D., 1986. Coupled trace element and isotope enrichment in the Cook–Austral–Samoa islands, southwest Pacific. *Earth Planet. Sci. Lett.* 79 (3–4), 270–280.
- Paulick, H., Munker, C., Schuth, S., 2010. The influence of small-scale mantle heterogeneities on Mid-Ocean Ridge volcanism: Evidence from the southern Mid-Atlantic Ridge (7°30'S to 11°30'S) and Ascension Island. *Earth Planet. Sci. Lett.* 296 (3–4), 299–310.
- Polyakov, A.I., Bagdasar'yan, G.P., 1986. The age of young volcanoes in East Siberia and regularities of the composition evolution of volcanics. *Geokhimiya*, No. 3, 311–317.
- Putirka, K.D., 2008. Thermometers and barometers for volcanic systems. *Rev. Mineral. Geochem.* 69 (1), 61–142.
- Rasskazov, S.V., 1987. Plutonic inclusions from Late-Cenozoic melanephelinites in the southern part of Central Transbaikalia. *Geologiya i Geofizika (Soviet Geology and Geophysics)* 28 (7), 50–60 (44–53).
- Rasskazov, S.V., Saranina, E.V., Demonterova, E.I., Maslovskaya, M.N., Ivanov, A.V., 2002. Mantle components in Late Cenozoic volcanics, East Sayan (from Pb, Sr, and Nd isotopes). *Geologiya i Geofizika (Russian Geology and Geophysics)* 43 (12), 1065–1079 (1014–1028).
- Rudge, J.F., Reynolds, B.C., Bourdon, B., 2009. The double spike toolbox. *Chem. Geol.* 265, 420–431.
- Saibatalova, E.V., Kulikova, N.N., Sutin, A.N., Paradina, L.F., Pakhomova, N.N., Vodneva, E.N., Semiturkina, N.A., 2010. Influence of sample preparation on the determination of the elemental composition of fresh water sponges by inductively coupled plasma mass spectrometry. *J. Anal. Chem.* 65 (7), 674–681.
- Samsonova, N.S., 1973. Nepheline Group Minerals [in Russian]. Nauka, Moscow.
- Savatenkov, V.M., Yarmolyuk, V.V., Kudryashova, E.A., Kozlovskii, A.M., 2010. Sources and geodynamics of the Late Cenozoic volcanism of Central Mongolia: evidence from isotope-geochemical studies. *Petrology* 18 (3), 278–307.
- Shaw, C.S.J., Dingwell, D.B., 2008. Experimental peridotite–melt reaction at one atmosphere: a textural and chemical study. *Contrib. Mineral. Petrol.* 155 (2), 199–214.
- Skolotnev, S.G., 2014. New isotopic data for Mid-Atlantic Ridge basalts from the Arkhangelsk–Sierra Leone fracture zone (central Atlantic). *Dokl. Earth Sci.* 459 (1), 1429–1435.
- Sobolev, A.V., Hoffman, A.W., Sobolev, S.V., Nikogosian, I.K., 2005. An olivine-free source of Hawaiian shield basalts. *Nature*, 434 (7033), 590–597.
- Sobolev, A.V., Hoffman, A.W., Kuzmin, D.V., Yaxley, C.M., Arndt, N.T., Sun-Lin Chung, Danyushevsky, L.V., Elliot, T., Frey, F.A., Garcia, M.O., Gurenko, A.A., Kamenetsky, V.S., Kerr, A.C., Krivolutsкая, N.A., Matvienkov, V.V., Nikogosian, I.K., Rocholl, A., Sigurdsson, A., Sushchevskaya, N.M., Teklay, M., 2007. Amount of recycled crust in sources of mantle-derived melts. *Science* 316 (5823), 412–417.
- State Geological Map of the Russian Federation, Scale 1: 1,000,000 (Third Edition). Aldan–Transbaikalian Series. Sheet M-49: Petrovsk-Zabaikal'skii. Explanatory Note [in Russian], 2012. Kartograficheskaya Fabrika VSEGEI, St. Petersburg.
- Stracke, A., 2012. Earth's heterogeneous mantle: a product of convection-driven interaction between crust and mantle. *Chem. Geol.* 330–331, 274–299.
- Sun, S.-S., McDonough, W.F., 1989. Chemical and isotopic systematics of oceanic basalts: implication for mantle composition and processes, in: *Magmatism in the Ocean Basins*. *Geol. Soc. London, Spec. Publ.* 42, Blackwell Scientific Publications, pp. 313–346.
- Tsybukova, S.S., Perepelov, A.B., Demonterova, E.I., Pavlova, L.A., Travin, A.V., Puzankov, M.Yu., 2014. Origin and evolution of Neogene alkali-basaltic magmas in the southwestern flank of the Baikal rift system (Heven lava plateau, northern Mongolia). *Russian Geology and Geophysics (Geologiya i Geofizika)* 55 (2), 190–215 (244–275).
- Vorontsov, A.A., Yarmolyuk, V.V., 2004. North-Mongol–Transbaikalia polychronic rift system (stages of formation, magmatism, sources of melts, geodynamics). *Litosfera*, No. 3, 17–32.
- Wang, Y., Han, B., Griffin, W.L., Zhang, L., Shu, G., 2012. Post-entrapment mineral–magma interaction in mantle xenoliths from inner Mongolia, western North China Craton. *J. Earth Sci.* 23 (1), 54–76.
- Weaver, B.L., 1991. The origin of ocean basalt end-member composition: trace element and isotopic constraints. *Earth Planet. Sci. Lett.* 104 (2–4), 381–397.
- Workman, R.K., Hart, S.R., Jackson, M., Regelous, M., Farley, K.A., Blusztajn, J., Kurz, M., Staudigel, H., 2004. Recycled metasomatized lithosphere as the origin of the Enriched Mantle II (EM-2) end-member: Evidence from the Samoan Volcanic Chain. *Geochem. Geophys. Geosyst.* 5 (4), Article Q04008, doi:10.1029/2003GC000623.
- Yarmolyuk, V.V., Kovalenko, V.I., Ivanov, V.G., 1995. Late Mesozoic–Cenozoic intraplate volcanic province in Central–East Asia, a projection of the hot mantle field. *Geotektonika*, No. 5, 41–67.
- Yarmolyuk, V.V., Ivanov, V.G., Kovalenko, V.I., 1998. Sources of the late Mesozoic–Cenozoic intraplate magmatism in western Transbaikalia (from geochemical and isotope data). *Petrologiya* 6 (2), 115–139.
- Yarmolyuk, V.V., Lebedev, V.I., Sugorakova, A.M., Bragin, V.Yu., Litasov, Yu.D., Prudnikov, S.T., Arakelyants, M.M., Lebedev, V.A., Ivanov, V.G., Kozlovskii, A.M., 2001. The East Tuva area of recent volcanism in Central Asia: stages, products, and type of volcanic activity. *Vulkanologiya i Seismologiya*, No. 3, 3–32.
- Yarmolyuk, V.V., Ivanov, V.G., Kovalenko, V.I., Pokrovskii, B.G., 2003. Magmatism and geodynamics of the Southern Baikal volcanic region (mantle hot spot): results of geochronological, geochemical, and isotopic (Sr, Nd, and O) investigations. *Petrology* 11 (1), 1–30.
- Yarmolyuk, V.V., Kudryashova, E.A., Kozlovskiy, A.M., Savatenkov, V.M., 2011. Late Cenozoic volcanic province in Central and East Asia. *Petrology* 19 (4), 327–347.
- Zartman, R.E., Doe, B.R., 1981. Plumbotectonics – the model. *Tectonophysics* 75 (1–2), 135–162.
- Zindler, A., Hart, S., 1986. Chemical geodynamics. *Ann. Rev. Earth Planet. Sci.* 14, 439–571.
- Zolotukhin, V.V., Al'mukhamedov, A.I., Medvedev, A.Ya., 1996. Modeling of primary melt for tholeiites of Siberian and Deccan basalts. *Gondwana Geol. Mag.* 2, 283–291.
- Zorin, Yu.A., Rogozhina, V.A., 1978. Mechanism of rifting and some features of the deep-seated structure of the Baikal rift zone. *Tectonophysics* 45 (1), 23–30.
- Zorin, Yu.A., Novoselova, M.R., Turutanov, E.Kh., Kozhevnikov, V.M., 1990. Structure of the lithosphere of the Mongolian–Siberian mountainous province. *J. Geodyn.* 11 (4), 327–342.